Applied Energy 349 (2023) 121610

Contents lists available at ScienceDirect

Applied Energy

journal homepage: www.elsevier.com/locate/apenergy

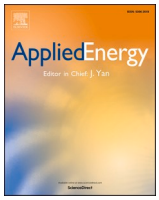

Comprehensive analysis of thermal runaway and rupture of lithium-ion batteries under mechanical abuse conditions

Haodong Chen [a,*], Evangelos Kalamaras [a,b], Ahmed Abaza [c], Yashraj Tripathy [a,b], Jason Page [c], Anup Barai [a,*]

[a] WMG, University of Warwick, Coventry CV4 7AL, UK
[b] The Faraday Institution, Quad One, Harwell Campus, Didcot OX11 0RA, UK
[c] Jaguar Land Rover Limited, Whitley, Coventry CV3 4LF, UK

HIGHLIGHTS

- Temperature, residual mass, fire behaviour and voltage change were characterised.
- Effects of test parameters on thermal runaway and rupture were investigated.
- Likelihood of both thermal runaway and rupture with respect to testing parameters were evaluated.
- A triangle of factors affecting sidewall rupture of lithium-ion batteries was proposed.
- X-ray computed tomography of internal structure of cells after thermal runaway.

ARTICLE INFO

Keywords:
Battery safety
Thermal runaway
Nail penetration
Sidewall rupture
Computed tomography

ABSTRACT

Sidewall rupture of lithium-ion batteries plays an important role in thermal runaway (TR) propagation because flame burst from the side of cell can directly heat adjacent cells. However, the understanding of sidewall rupture in high specific energy cells under mechanical abuse conditions remains limited. In this work, nail penetration is adopted as a trigger method of TR of 21700-format cylindrical cells with high specific energy (257.0 W•h/kg). The effects of test parameters including nail diameter, nail speed, penetrating location, penetrating depth, and state of charge on likelihood and severity of thermal runaway and sidewall rupture behaviour were investigated. A series of equipment including high-definition cameras, thermal imaging camera, X-ray computed tomography (CT), cycler and electronic balance were adopted to reveal the behaviour and the mechanism of TR and sidewall rupture. Discussion on CT scan and fire behaviour provides new perspectives for understanding sidewall rupture and TR mechanisms in high specific energy cells. The results show that the mean mass loss ratio of the cell with 100% SoC is greater than 45% under each test condition, and the maximum of them is as high as 62.5% when penetrating off-centre from the cell bottom and with a penetrating depth of 10 mm. The likelihood of sidewall rupture increases with the increasing nail speed, nail diameter, penetrating depth and state of charge when penetrating from the top cover of the cell, but it is little affected by the penetrating depth and nail diameter for penetrating from the bottom of the cell. For the first time such a relationship is presented. The root-cause analysis for the sidewall rupture of the cell has been discussed, which highlights the three key factors, including the casing strength, the internal pressure, and the opening area of the venting disk.

1. Introduction

Road electric vehicles (EVs) powered by lithium-ion batteries (LIBs) have proven to be safer than their gasoline-powered counterparts [1]. Following their success in the automotive industry, LIBs are being considered for a new generation of all-electric aircraft. For example, Norway and Sweden previously mandated that all short-haul flights be fully electric by 2040 [2]. In the UK, Aerospace Technology Institute (ATI) has published the technology strategy [3], highlighting the emergence of an entirely new aviation market in the sub-regional and

* Corresponding authors.
E-mail addresses: Haodong.chen@warwick.ac.uk (H. Chen), a.barai@warwick.ac.uk (A. Barai).

https://doi.org/10.1016/j.apenergy.2023.121610
Received 17 April 2023; Received in revised form 1 July 2023; Accepted 13 July 2023
Available online 3 August 2023

Table 1
Summary of some typical nail penetration tests from reference.

Format	Cathode/ anode	Capacity (Ah)	Specific energy (W•h/kg)	Nail diameter (mm)	Nail speed (mm/s)	Key indicator	Main finding	Note	Ref.
Cylindrical cell 18650	NMC-LCO/ graphite; LFP/ graphite	2.6/1.1	204.7/ 93.1	3	80	Temperature on cell surface, residual mass, and chamber pressure	Cells with the LFP cathode and PP-PE-PP separator shows much better safety performance than cells with the NMC-LCO cathode and PE separator. The maximum temperature range is from 101.48 °C to 105.50 °C, and weight loss range is from 3.48% to 4.78% for LFP cells at 50% SoC.	Various battery chemistries and separator types	[31]
	NMC/ graphite	2.2	168.5	4	Not given	Internal temperature and surface temperature	The maximum internal temperature is higher than 900 °C, which is around 300 °C greater than the surface temperature. The maximum internal temperature range is from 672 °C to 920 °C, and the maximum surface temperature measured by a thermal camera is 455–610 °C. Internal structure evolution observed by a high-speed synchrotron X-ray radiography	Various penetrating positions	[43]
	NMC-LMO/ graphite	2.0	168.2	3	20/30/ 40	Temperature on cell surface and residual mass	The outcome of TR events increases with the increasing SoC; penetrating at side centre is the most dangerous case. The maximum temperature for 100% SoC cells with pierced penetration is 465.8 ± 51.4 °C and the residual mass is 31.42 ± 1.02 g.	Various SoCs, penetrating locations, and penetrating depths	[28]
	NMC/ graphite	2.58	Not given	6	0.1/ 10/100	Temperature on cell surface and cell voltage	The outcome of TR increases with the increasing nail speed, and the maximum temperature increases from 466.8 °C to 695.6 °C from the low nail speed to the high nail speed.	Various nail speeds	[27]
	LFP/ graphite	1.5	135.0	3/5/8	10/20/ 20/40	Temperature on cell surface and cell voltage	The risk of TR increases with the increasing SoC; the occurrence of TR depends on the penetrating depth, and the maximum temperature range is from 131.8 °C to 135.9 °C for 100% SoC cells penetrating with different nail diameters.	Various SoCs, penetrating locations, nail diameters, and penetrating depths	[37]
Pouch cell	LMO-NMC/ graphite	15.0	Not given	10	100	Temperature on cell surface and cell voltage	Poor reproducibility using conductive nails; a clear distinction between the outcome of the conductive and non-conductive nails. The maximum temperature is 112.9 °C for hard short circuit (0.562 mΩ) and drops to 67.7 °C for soft short circuit (24.0 mΩ).	Various nail materials (Copper/steel/ plastic)	[24]
	LCO/ graphite	0.06/ 0.42 /0.86	Not given	5	3	Cell voltage	Observation of internal structure evolution during test	Various capacities and nail speeds	[34]
	LNCO-LCO/ graphite	5.5	169.6	3	1/5/ 10/40/ 80	Temperature on cell surface, cell voltage, and released gases	Good reproducibility generated by combining low nail speed (1 mm/s) and a conductive nail. The maximum temperature range is from 479.49 °C to 503.95 °C and from 438.17 °C to 471.42 °C for conductive nail and non-conductive nail, respectively.	Various nail materials (Stainless steel/ zirconium oxide), nail speeds, and penetrating depths	[25]
	LNCO-LCO/ graphite	3.7/5.7	204.3/ 206.8	2/3/4/5	1	Temperature on cell surface, cell voltage, and released gases	No change for voltage drop, the development of temperatures and the infrared-active gas products when using different nail geometries. The peak concentration of methane is 3897 ± 217 mg/m^3 for the cell with 3.7 Ah and there are two peak concentrations of 3835 ± 222 mg/m^3 and 3569 ± 201 mg/m^3 for the cell with 5.7 Ah.	Various capacities and nail diameters	[36]

(*continued on next page*)

Table 1 (*continued*)

Format	Cathode/ anode	Capacity (Ah)	Specific energy (W•h/kg)	Nail diameter (mm)	Nail speed (mm/s)	Key indicator	Main finding	Note	Ref.
	NMC-LCO/ graphite-SiO_x	1.0	185.0	3/5/8	10/20/ 20/40	Temperature on cell surface, cell voltage	The cell with a higher SOC is easily triggered to TR by nail penetration with a thicker nail. The maximum temperature range is 98.0–105.5 °C for different nail speeds.	Various SoCs, penetrating locations, nail diameters, and penetrating depths	[29]

Note: LCO ($LCoO_2$); $LiFePO_4$ (LFP); $LiMn_2O_4$ (LMO); $LiNiCoO_2$ (LNCO); $LiNi_xMn_yCo_zO_2$ (NMC). References [24,25] adopt various nail materials, other references listed in this Table use a stainless steel nail.

urban environments by 2030, enabled by the full-electric propulsion system. In 2021, the UK Civil Aviation Authority (UK CAA) published the UK legislative framework towards net-zero aviation [4]. The realistic energy storage technology that can meet the power and energy density demands of this emerging electrified sector is lithium-ion and its future variants. However, irrespective of the fantastic safety record of LIB in automotive industry, aerospace organisations are uneasy about battery safety [5]. This is due to the fundamental premise of safety plus the need to monitor, identify and isolate or mitigate failure is different. Similar battery safety concern is still a major roadblock for other applications e.g. grid-connected energy storage system that contains a large number of LIBs [6–8].

When a large number of LIB cells are assembled into a pack, the major risk is thermal runaway (TR) propagation [9]. One of the leading cause of TR propagation is sidewall rupture of the cell, which directly affect the neighbouring cells, leading to a chain reaction [9,10]. The sidewall rupture behaviour previously reported in 18650-format cells [11–15] and prismatic cells [16]. Anderson et al. [11] found that 18650-format cylindrical cells with both thin wall thickness and high volumetric energy density have a high likelihood of sidewall rupture under oven heating conditions. Finegan et al. [13] investigated a reason leading to rupture of 18650-format cells under external heating and confirmed that the venting disk plays an important role in sidewall rupture. Lao et al. [10] proposed that a reduction in mechanical strength under high temperatures is a key factor leading to sidewall rupture. Chen et al. [17] found that the sidewall rupture is severer at high state of charge (SoC) for 21700-format cylindrical cells under radial nail penetration. In addition, Jia et al. [15] developed a physics-based model to simulate the deformation and fracture behaviours of 18650-format cells under laser heating. To the best of our knowledge, parametric study was mainly focused on 18650-format cells and some pouch cells of energy density lower than 200 W•h/kg, as shown in Table 1.

Although in a few cases external heating [11–15] and overcharge [16] were previously used to study sidewall rupture behaviour of 18650-format cylindrical cells and prismatic cells, the internal space of the cell is not greatly changed or fixed under these abuse test conditions. Nail penetration is commonly used as a trigger method of TR initiation [18,19] and TR propagation [20–22] and it is listed as one of the mechanical abuse tests in most international and national battery test standards [23]. In this work, nail penetration is adopted as a trigger method for studying the sidewall rupture behaviour because the internal short circuit of a cell is instantly generated after nail penetration and the penetrating nail can affect the internal space and further influences the internal pressure and rupture behaviour.

However, the outcome of TR during a nail penetration test is strongly influenced by many factors such as nail material [24–26], nail speed [25,27–30], penetrating depth [25,28], battery chemistry [31–33], capacity [34–36], SoC [28–30,37], short resistance [38,39], etc. As shown in Table 1, a stainless steel nail is commonly used by researchers, in addition, other conductive materials such as copper [24] and non-conductive materials [25,26] are also adopted by researchers. The nail diameter recommended is 3 mm for cell level on the international standard SAE J2464 [40] and from 3 mm to 8 mm on the Chinese standard GB 38031–2020 [41]. Other nail sizes were also used, such as 10 mm [24] and 2 mm [36] as well as very thin nail-like needles [35]. The nail speed recommended is at least 80 mm/s on the international standard SAE J2464 [40] and 0.1 mm/s ~ 10 mm/s on the Chinese standard GB 38031–2020 [41]. Lower nail speed as slow as 1 mm/min was also adopted by researchers [42]. However, a comprehensive analysis of impact of the nail speed on high specific energy cells (≥250 W•h/kg) has not been performed yet. Also, it can be seen from Table 1, the single variable parameter such as nail material is investigated in some references [24, 27, 43]. Detailed studies on variable parameters were performed in the cylindrical cells with small capacity and low specific energy of less than 170 W•h/kg [28]. In addition, an electrochemical-thermal coupled model [18,26,30,38,39,42,44–49] was developed to simulate the electrochemical and TR behaviour of LIBs during nail penetration tests and to perform the parametric study of both nail and cell based on the porous electrode theory [50,51] and thermal abuse reaction models [52,53], but not focused on here.

In recent years, high energy density (>250 W•h/kg) cylindrical cells such as 21700-format have been commercially adopted by automotive manufacturers. This cell format is also currently being considered for the electric propulsion systems for electric aircraft. Compared to 18650-format cells, the energy stored in the 21700-format cell is higher by around 50% [54]. High specific energy means a high risk of thermal runaway event. The failure mode and the failure mechanism of cells with high specific energy therefore likely be different from low specific energy cells. For example, violent jet fire behaviour of 21700-format cells was reported in our previous study [55], and the sidewall rupture behaviour of 21700-format cells under external heating and nail penetration were often observed [10,17,56]. The 21700-format cells have the same housing materials and wall thicknesses as 18650-format cells. However, inside a 21700 cell, higher amount of gas generation is expected than 18650-format cells, which will increase the internal pressure of the cell compared to the cells with similar size but lower specific energy. In tandem with the pressure increase, the expected higher heat generation will increase the cell temperature at a higher rate. The strength of the cell casing reduces significantly when temperature increases [10]. These two mechanisms likely will translate into sidewall rupture and a more violent TR outcome. However, the understanding of TR and sidewall rupture behaviour of high specific energy cells such as 21700-format under mechanical abuse remains limited. Therefore, it is necessary to investigate the behaviour of TR and sidewall rupture of cells with high energy density under mechanical abuse and their influencing factors for the deep understanding of the mechanism of TR and sidewall rupture.

This work aims to establish the detailed relationship between sidewall rupture and penetrating parameters. Also, this work will fill the gap of parametric study on high specific energy cells under mechanical abuse conditions. Commercial 21700-format cells with high specific energy (257.0 W•h/kg) are adopted and nail penetration is used as a trigger method for the mechanical abuse. Effects of SoC, nail diameter, nail speed, penetrating location, and penetrating depth on behaviours of

Table 2
Battery information.

Item	Specification/value	Unit
Format	21700	–
Rated capacity	4.8	Ah
Mass	67.5 ± 1.5	g
Nominal voltage	3.62	V
Charge cut-off voltage	4.2	V
Discharge cut-off voltage	2.5	V
Operating temperature	Charge: 0 to 45 Discharge: −30 to 60	°C
Cathode	Lithium nickel cobalt aluminium oxide	–
Anode	Graphite and Si	–

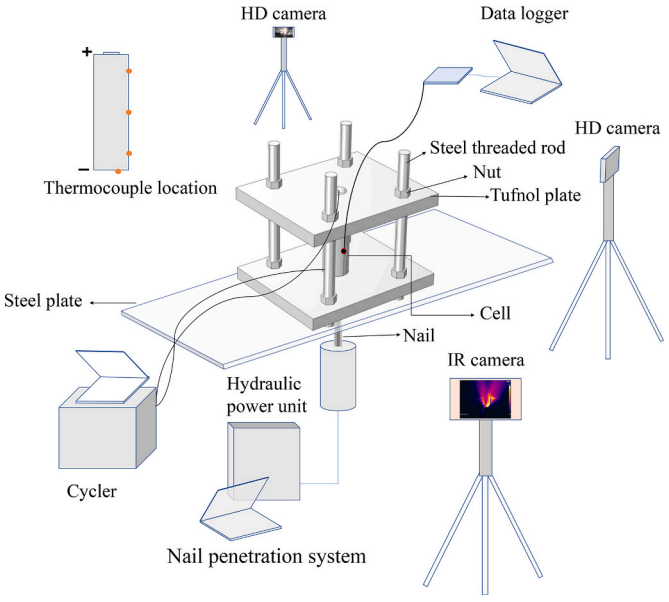

Fig. 1. Schematic diagram of the test apparatus and thermocouple location, reproduced from Ref. [17].

TR and sidewall rupture are investigated by a combination of many tools such as a nail penetration system, optical cameras, a thermal imaging camera, X-ray CT, and an electronic balance.

2. Experiments

2.1. Battery information

In these tests, commercial 21700-format LIBs from the same manufacturer and same production batch with lithium nickel cobalt aluminium oxide cathode and graphite and Si anode were chosen due to its higher specific energy of 257 W•h/kg. As listed in Table 2, the rated capacity of the cell is 4.8 Ah, and the nominal voltage is 3.62 V. The charge cut-off voltage and discharge cut-off voltage are 4.2 V and 2.5 V, respectively. The mass of the cell is 67.5 ± 1.5 g. The venting disks includes two parts: the bottom disk and the top disk. There are six peripheral holes and one centre hole on the bottom disk and a pre-set scoring on the top disk, which provides a gas pathway when it breaks under a high internal pressure.

2.2. Test setup

A schematic diagram of cell, cell holder and experimental setup is shown in Fig. 1. The naked cell was fixed by a cell holder made of Tufnol material using screws and nuts and the cell holder, which was fastened to the hydraulic nail penetration system using jigs. Four type K thermocouples located at 10 mm from the cell base, in the middle of cell, 10 mm from the cell top, and the cell bottom, respectively, are displayed in Fig. 1 for measuring the temperatures on cell surface. All temperatures were recorded by a data logging software (PicoLog, UK) with a time interval of 10 ms. Two high definition (HD) cameras recording at 30 frames per second were placed in the front of the cell with 0.72 m and side of cell with 0.44 m, respectively, to capture the TR behaviours during tests. One infrared radiation (IR) camera (FLIR T640, USA) recording at 30 frames per second was positioned at a stand-off distance of 1.52 m from the back of the cell to capture temperature evolution on the cell surface.

Table 3
Summary of test conditions.

Test condition no.	Penetrating location	Nail parameter and cell SoC	Variable	Value	Number of cells	CT scan
1	Penetrate from the middle of the top cover of the cell*	Nail diameter: 4 mm, nail speed: 6 mm/s	SoC	100% SoC	6	
2				92% SoC	5	
3				70% SoC	5	
4				50% SoC	5	
5				30% SoC	3	
6				0% SoC	3	
7		Nail speed: 6 mm/s, 100% SoC	Nail diameter	3 mm	5	No. 1**
8				8 mm	6	
9		Nail diameter: 4 mm, 100% SoC	Nail speed	0.5 mm/s	5	No. 1
10				100 mm/s	5	No. 4
11	Penetrate from the bottom of the cell	Nail diameter: 4 mm, nail speed: 6 mm/s, 100% SoC	Insertion depth (Bottom centre)	Not specified*	5	
12				20 mm (Nail diameter: 8 mm)	4	No. 3
13		Nail diameter: 4 mm, nail speed: 6 mm/s, 100% SoC	Insertion depth (Bottom centre)	10 mm	3	
14				20 mm	3	No. 3
15				30 mm	3	
16		Nail diameter: 4 mm, nail speed: 6 mm/s, 100% SoC	Insertion depth (Off-centre)	5 mm	5	
17				10 mm	5	No. 1

* Note: the nail was stopped when sparks were observed.
** Note: No. 1 means that the first test used for CT scan after TR test in this group.

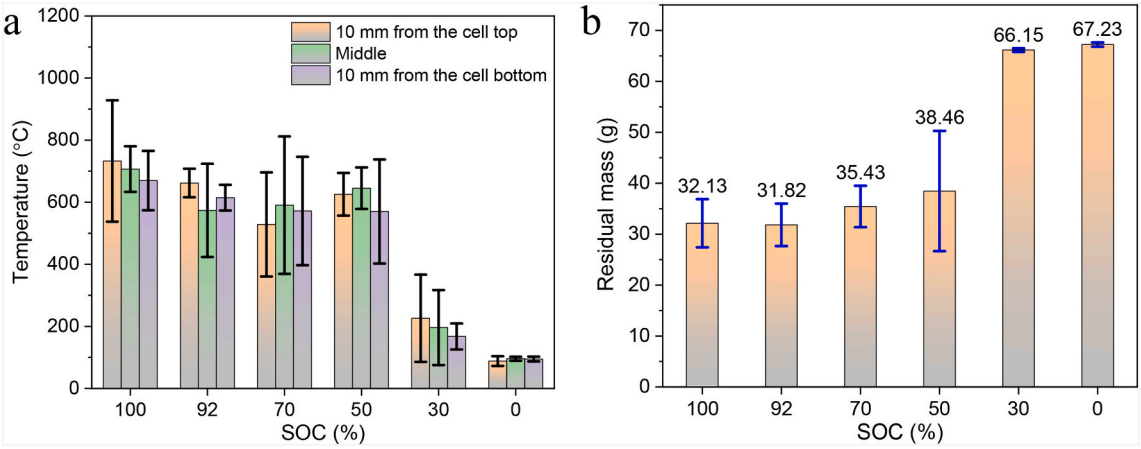

Fig. 2. Comparison of (a) the mean maximum temperature at different measuring points and (b) the mean residual mass of the cell with various SoCs.

2.3. Test procedure

All cells were firstly charged to 100% SoC and then rest for half an hour, and next discharged to desired SoC with 1C (4.8 A) discharging current rate and finally rest for at least 1 h before tests. All cells were pierced by a nail made of stainless steel with a conical tip of 40° and various diameters penetrating depths, and speeds, which was controlled by the penetration test control system. The test procedure is as follows:

(1) Charge cells to 100% SoC, then discharge to desired SoC;
(2) Put thermocouples on cell surface, then place the cell into the cell holder;
(3) Fix the cell with screws and nuts, and clamp the cell holder using G-shape clamps;
(4) Connect data logger, cycler, cameras to laptops with USB cables;
(5) Set penetrating parameters and run a test.

Test conditions are summarised in Table 3. Five different parameters i.e., SoC, nail diameter, nail speed, penetrating depth and penetrating location were studied. For each testing condition, at least 3 repeat tests were performed. A total of 76 tests were conducted and 6 cells were CT scanned after test. The selection of nail parameters was referred to the Chinese standard GB 38031–2020 [41].

3. Results and discussion

3.1. Effect of SoC

As shown in test conditions 1–6, various SoCs from 0% SoC to 100% SoC were adopted to investigate the effect of SoC on TR behaviour and sidewall rupture of the cell in this work. The key TR indicators are defined as follows. The maximum temperature is the measured maximum temperature of repeated tests at all measuring points on cell surface. The mean maximum temperature is the mean of measured maximum temperature of repeated tests at the same measuring point on cell surface. The residual mass is the mass of the cell after test, measuring by an electronic balance with an accuracy of 0.1 g. The mean residual mass is the mean of measured mass of the cell after test of repeated tests. The mean mass loss ratio is the mean of mass loss of the cell of repeated tests compared with the original mass. The mean maximum temperature at different measuring points and the mean residual mass after test are plotted in Fig. 2a and Fig. 2b, respectively. The mean maximum temperature at different measuring points on cell surface is not greatly affected by the SoC for tests at the SoC no less than 50%, while it decreases with the decreasing SoC for tests at the lower SoC ($\leq$ 30% SoC) due to less Joule heat generated inside the cell. According to temperatures recorded by thermocouples, the maximum temperature on cell surface of the test at the SoC no less than 50% is higher than 680 °C, while it is less than 390 °C for the test at the lower SoC ($\leq$ 30% SoC). It is because those tests at the SoC no less than 50% experienced TR, but the lower SoC ($\leq$ 30% SoC) cells did not go into TR, showing sparks and smoke but without fire in one test at 30% SoC, and little smoke or no smoke in other tests. As shown in Fig. 2b, the mean residual mass is not greatly affected by the SoC no less than 92%, but it increases with the decrease in SoC ($\leq$ 92% SoC). The mean mass loss ratio of the cell with 100% SoC is up to 52.4%, which means approximately 52.4% of battery mass ejected outside the cell. It suggests that more battery components were ejected during the test at the high SoC. Combining the maximum temperature on cell surface and the residual mass, the results show that the severity of TR increases with the increasing SoC. From the view of heat generation and thermal stability of material, the reason can be summarized as follows: 1) more Joule heat is generated for high SoC cells because more energy stored in the active materials for high SoC cells will flow through the nail after nail pierces electrode layers, and 2) the thermal stability of anode materials reduces at high SoC due to increased lithiation in anode [28,57]. Therefore, it is easier to trigger chain reactions of TR for high SoC cells. The current results confirmed that the severity of TR events increases with the increasing SoC reported by some researchers [28,31].

The TR behaviour for tests at 50% SoC was observed in this work, but it was not found in 18650-format cells at 50% SoC and even one test at 70% SoC [28]. The mean maximum temperature and mean mass loss ratio of 100% SoC cells in this work are higher by ~57% and ~83% compared to 18650-format cells at 100% SoC reported by Mao et al. [28], separately. Note that the penetrating position in their study is different from this work. The 18650-format cells were triggered to TR under radial penetration in their work [28], while in this work the cells were triggered to TR under longitudinal direction. Our previous study showed that the 21700-format cells are easily to trigger to TR and sidewall rupture under radial direction compared with that under longitudinal direction [17]. It is worth mentioning that the specific energy of the 21700-format cell in this work is higher by ~53% compared to 18650-format cells reported by Mao et al. [28]. The fire behaviour discussed in Section 3.6 is also more violent than that reported by Mao et al. [28].

Sidewall rupture was only observed in two of six cells tested at 100% SoC, not at other SoCs. It suggests that it is easier to cause sidewall rupture for cells at 100% SoC than other SoCs. More cells occurred sidewall rupture in our study under different testing conditions, while the rupture behaviour was not reported by Mao et al. [28] in 18650-

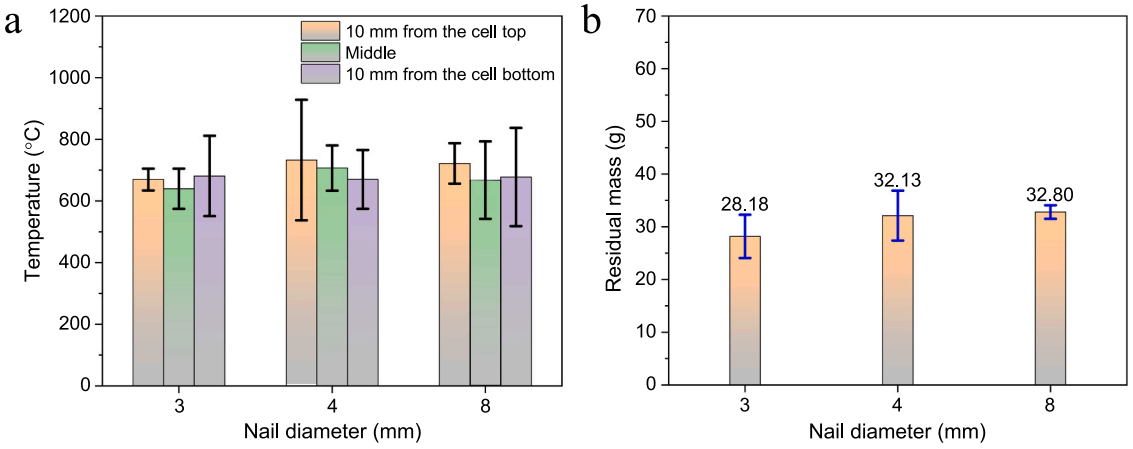

Fig. 3. Comparison of (a) the mean maximum temperature at different measuring points and (b) the mean residual mass of the cell penetrated at different nail diameters.

Fig. 4. Photos after test penetrated at different nail diameters. (a) 3 mm, (b) 4 mm and (c) 8 mm.

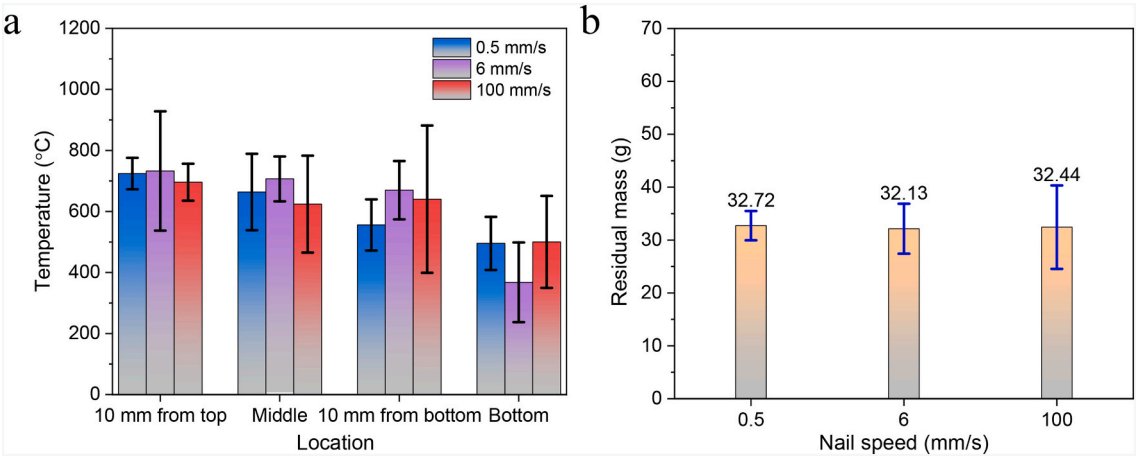

Fig. 5. Comparison of (a) the mean maximum temperature at different measuring points and (b) the mean residual mass of the cell penetrated at different nail speeds.

format cells. The reason of sidewall rupture will be discussed in Section 3.7. Combining the four indicators of the maximum temperature on cell surface, the residual mass, fire behaviour, and the rupture behaviour, the present results indicate that the TR of cells with high specific energy is more violent than that with low specific energy cells.

3.2. Effect of nail diameter

As shown in test conditions 1, 7 and 8, three different nail diameters, 3 mm, 4 mm, and 8 mm were adopted to investigate the effect of nail diameter on TR behaviour and sidewall rupture of the cell in this work. The mean maximum temperature at different measuring points on cell surface and the mean residual mass after test are plotted in Fig. 3a and Fig. 3b, respectively. The results show that the mean maximum temperature at different measuring points on cell surface is little influenced by the nail diameter. The similar results were also reported by Doose et al. [36] and Huang et al. [37] using pouch cells with different capacities and 18650-format cells with the LFP cathode, respectively. The possible reasons lie in the following two aspects: 1) a thick nail means a large short-circuit area and a low short-circuit resistance, therefore a high current can flow through the nail, and therefore more heat is generated, and 2) thick nail at the same time means large cross section, and more heat can be dissipated. These two effects offset each other, as a result there is no great difference on the average maximum temperature on cell surface when penetrating with different nail diameters. The mean mass loss ratio of the cell with 100% SoC is as high as 58.3% and 51.4% when penetrating with a 3-mm-nail diameter and an 8-mm-nail diameter, respectively. The mean residual mass of cell penetrated with a nail diameter of 3 mm is less than that penetrated with a nail diameter of 4 mm shown in Fig. 3b, but the difference is within the error bars. There is no great difference between tests penetrated with the 4-mm-nail diameter and the 8-mm-nail diameter.

As can be seen from Fig. 4, the cells with a large opening are exploded because a lot of pressure is accumulated inside the cell until the internal pressure exceeds the strength of the cell casing. Cracks in the cell casing possibly initiates in the lower part close to the cell bottom and propagates almost straight towards the top and the bottom of the cell. Although the effect of nail diameter on mean maximum temperature on cell surface was negligible, the sidewall rupture of cell was greatly influenced by the nail diameter. The thick nail can take up more space inside the cell than the thin nail, hence, the internal pressure of the cell penetrated by a thick nail is higher than that penetrated by a thin nail based on the idea gas law under the assumption of constant temperature and constant amount of substance. The present results show that nail diameter is a leading factor to cause sidewall rupture of the cell when penetrating from the middle of the top cover of the cell. The likelihood of sidewall rupture increases with the increasing nail diameter. For the first time such a relationship is presented, the mechanism of sidewall rupture will be discussed in detail in Section 3.7 combined with CT scan results.

3.3. Effect of nail speed

Three different nail speeds, 0.5 mm/s, 6 mm/s, and 100 mm/s were adopted to investigate the effect of nail speed on TR behaviour and

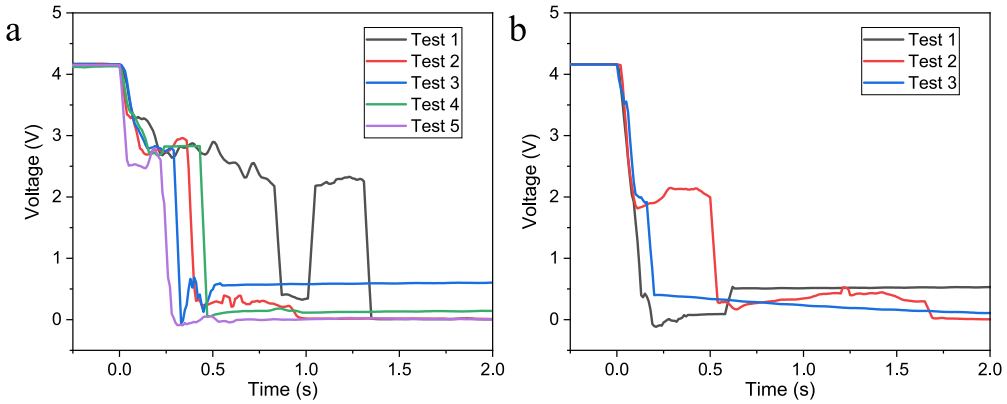

Fig. 6. Voltage profile of the cell penetrated from the top cover of the cell at a speed of (a) 0.5 mm/s, and (b) 100 mm/s.

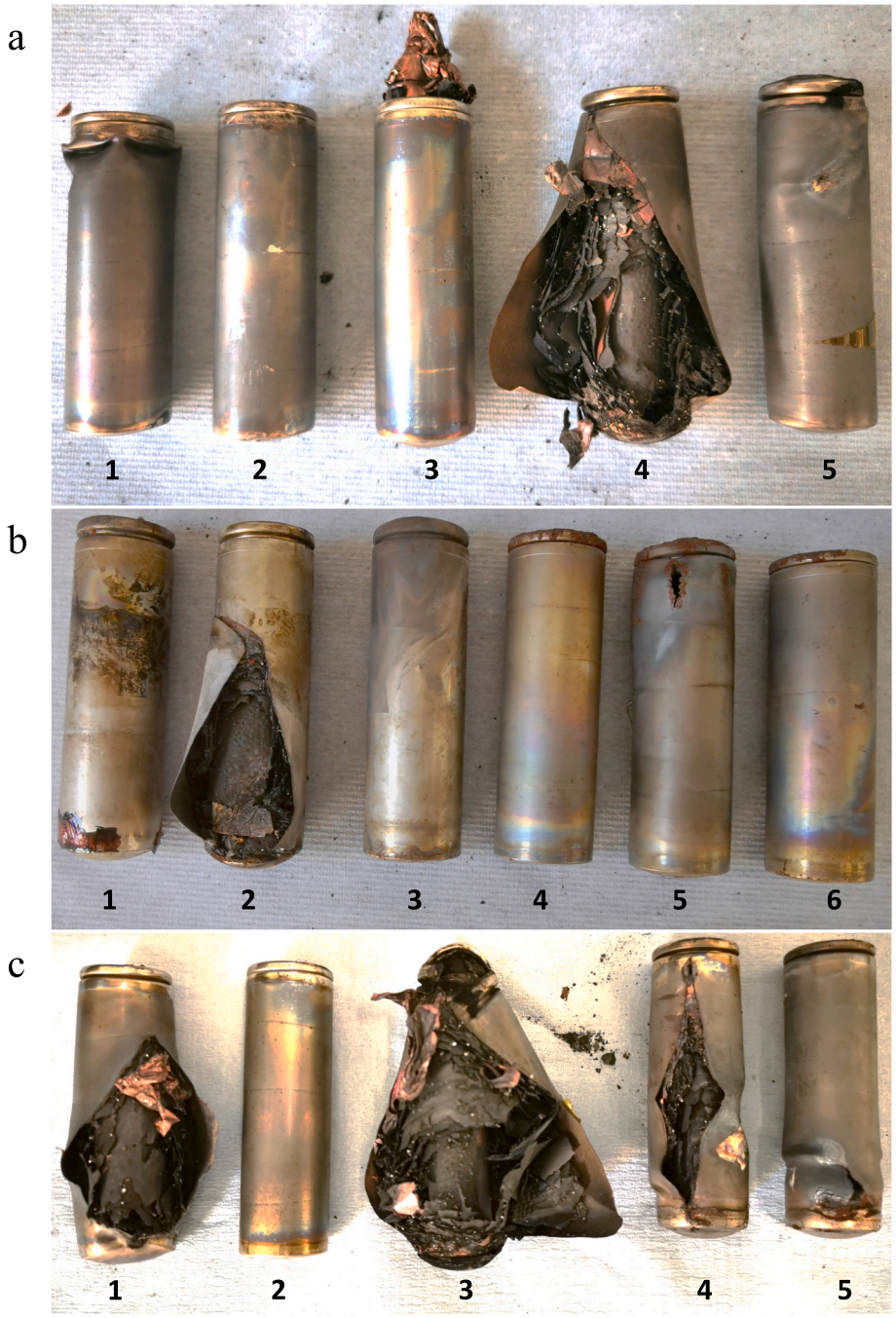

Fig. 7. Photos after test penetrated at different nail speeds. (a) 0.5 mm/s, (b) 6 mm/s, and (c) 100 mm/s.

sidewall rupture of the cell in this work (test conditions 1, 9 and 10). The mean maximum temperature at different measuring points on cell surface and the mean residual mass after test are presented in Fig. 5a and Fig. 5b, respectively. The high standard deviation of the mean maximum temperature at different measuring points on cell surface means that they are more spread out and are possibly influenced by the flame. The mean mass loss ratio of the cell with 100% SoC is as high as 51.5% and 51.9% when penetrating at a speed of 0.5 mm/s and 100 mm/s, respectively. The present results show that the mean maximum temperature on cell surface and mean residual mass of the cell after test are not greatly influenced by the nail speed. The same effect was reported by some researchers [28,29]. However, the peak of average temperature at 40 mm/s is higher than that at lower speeds (10–30 mm/s) reported by Huang et al. [37] with 18650-format LFP cells. The outcome of TR increases with the increasing nail speed from 0.1 mm/s to 100 mm/s reported by Ma et al. [27] with 18650-format NMC cells, but there are no repeat tests in their study. Fig. 6 shows the voltage profile of the cell penetrated from the top cover of the cell at different speeds. The moment when voltage starts to drop was set as zero for alignment. The voltage dropped rapidly to zero after nail penetration because internal short circuit was generated. As expected, testing at a speed of 100 mm/s required less time for the voltage to drop to zero compared to 0.5 mm/s.

As shown in Fig. 7, sidewall rupture occurs in one of the five tests penetrated at a speed of 0.5 mm/s, in two of the six tests penetrated at a

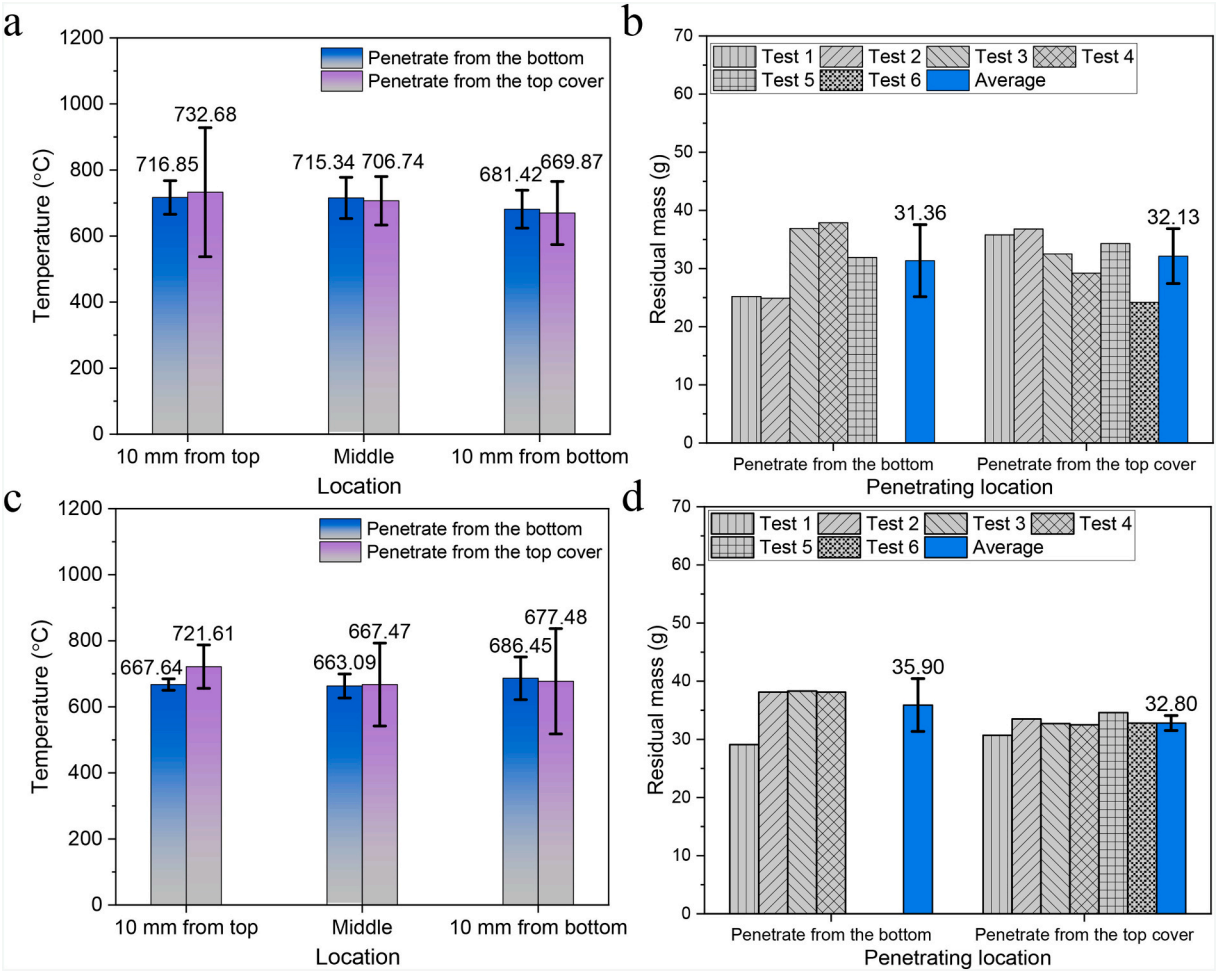

Fig. 8. Comparison of the mean maximum temperature at different measuring points and the mean residual mass of the cell penetrated at different locations. (a) and (b) nail diameter: 4 mm; (c) and (d) nail diameter: 8 mm.

speed of 6 mm/s, and in four of the five tests penetrated at a speed of 100 mm/s, respectively. The present results show that the nail speed is also a leading factor to cause sidewall rupture of the cell. The likelihood of sidewall rupture increases with the increasement of nail speed. The possible reasons are as follows: 1) at higher speed heat and gas are generated within a shorter period, and 2) more internal space is occupied by a higher-speed nail in a short time.

3.4. *Effect of penetrating location*

Two penetrating locations, from the top cover of the cell and from the bottom of the cell were adopted to investigate the effect of penetrating location on TR behaviour and sidewall rupture of the cell in this work. The mean maximum temperature at different measuring points on cell surface and the mean residual mass after test are plotted in Fig. 8. Two nail diameters of 4 mm and 8 mm are considered here. As shown in Fig. 8a and c, the mean maximum temperature at different measuring points on cell surface is not greatly affected by the penetrating location and the nail diameter, but the test penetrated from the bottom of the cell has a low standard deviation. As shown in Fig. 8b and Fig. 8d, the penetrating location also has little influence on the mean residual mass after test with the 4-mm-nail diameter, while the mean of residual mass after test penetrated from the bottom with the 8-mm-nail diameter is higher than that penetrated from the top cover of the cell. The mean mass loss ratio of the cell with 100% SoC is as high as 53.5% and 46.8% when penetrating from the cell bottom and with a 4-mm-nail diameter and an 8-mm-nail diameter, respectively.

Fig. 9 presents photos after nail penetration test from the cell bottom. The venting disk of the cell was completely destroyed, and the top cover of the cell was partly melted by flame for tests without sidewall rupture. Melted aluminium pieces came from current collector can be found on the top cover of the cell displayed in Fig. 9c due to the high internal pressure. Note that cell No. 4 penetrated with a nail diameter of 4 mm occurred sidewall rupture. This phenomenon was less common as only one test penetrated from the bottom of the cell happened. As shown in Fig. 9a, the top cover of Cell 4 is still in a good condition and the top disk of the cell just shows a small melting area, mostly in good condition. It suggests that the venting disk was not activated during the test and the gases were accumulated inside the cell until the sidewall rupture happened. Combined with the test results of penetration from the top cover of the cell, the present results show that the test penetrated from the top cover of the cell is more likely to occur sidewall rupture than that penetrated from the bottom of the cell. The main reason is that the venting disk is damaged and therefore does not work when penetrating from the top cover of the cell.

3.5. *Effect of penetrating depth*

Three different penetrating depths, 10 mm, 20 mm, and 30 mm, penetrated from the centre of the cell bottom (test conditions 13, 14 and 15) and two different penetrating depths, 5 mm, and 10 mm, penetrated off-centre from the cell bottom (test conditions 16 and 17) were adopted

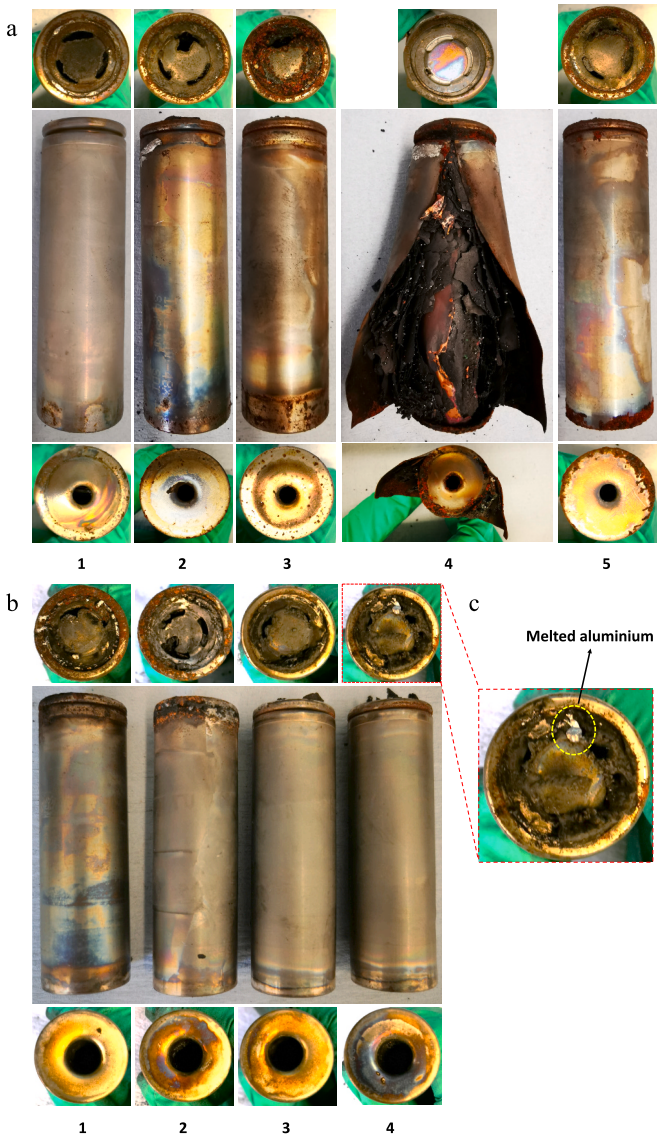

Fig. 9. Photos after tests penetrated from the cell bottom. Nail diameter: (a) 4 mm and (b) 8 mm, (c) enlarged view.

to investigate the effect of penetrating depth on TR behaviour and sidewall rupture of the cell in this work. The mean maximum temperature at different measuring points on cell surface and the mean residual mass after test are plotted in Fig. 10. The present results show that the mean maximum temperature on cell surface and the mean residual mass of cell after test are not greatly influenced by the penetrating depth when penetrating from the centre of the cell bottom. The mean mass loss ratio of the cell with 100% SoC is as high as 54.3%, 54.9%, and 51.2% when penetrating from the cell bottom centre and with a penetrating depth of 10 mm, 20 mm, and 30 mm, respectively. The mean maximum temperature at different measuring points on cell surface is also little influenced by the penetrating depth when penetrating off-centre from the cell bottom, but the mean residual mass after test with the 10-mm-penetrating depth is less than that with the 5-mm-penetrating depth. The mean mass loss ratio of the cell with 100% SoC is about 51.6% and 62.5% when penetrating off-centre from the cell bottom and with a penetrating depth of 5 mm and 10 mm, respectively. It means that TR of the cell with deeper insertion becomes more violent. Fig. 11 presents temperature profiles at different locations of 100% SoC cells penetrated off-centre from the cell bottom with penetrating depth of 10 mm. Temperature firstly rose to the peak value in a few seconds, then decreased gently because of cooling. Note that the thermocouple located 10 mm from the cell bottom of Test No. 5 in this group presented in Fig. 11c is failed in the test. As shown in Fig. 11, the temperature curves show a good repeatability. Fig. 12 shows the voltage profile of the cell during the test. The voltage dropped to zero in a very short time due to internal short circuit after penetration. Sidewall rupture was not observed in these tests. It further proves that penetrating from the top cover of the cell is easier to cause sidewall rupture than from the bottom of the cell.

3.6. Battery fire

Battery fire was observed during nail penetration tests in this work. The battery casing was firstly pierced, followed by damage to the electrode assembly. The internal short-circuit path was generated between cathode and anode electrode layers due to nail, and therefore a large amount of heat was released in a very short time. The heat generated would heat the penetrating region to high temperatures, which in turn initiated a series of exothermic reactions that produced a lot of flammable gases. Battery fire was created if these flammable gases were ignited by sparks. Fire behaviour of 18650-format cells under radial nail penetration was reported in previous literature [27,28]. The evolution of battery fire was described by Mao et al. [28], but only a narrow view of battery fire could be observed as the cell was inside an explosion-proof chamber. Ma et al. [27] also mentioned battery fire but without giving a detailed description. Only one camera was used to capture the battery fire in above references. As presented in above sections, the TR behaviour of 21700-format cells with a high specific energy becomes more violent than 18650-format cells.

According to our test results, all cells with a high SoC ($\geq$ 50%) experienced TR and occurred fire. There were only gases or smoke and sparks in tests at 30% SoC and only gases for 0% SoC tests. Two typical fire-burst behaviours were found based on cells with or without sidewall rupture. One is that the fire was only ejected from the top cover of the cell for cases without sidewall rupture, as presented in Fig. 13 and the other is that the fire was mainly ejected from the side of the cell for cases with sidewall rupture, as displayed in Fig. 14. The fire behaviour confirms that the outcome of TR for high energy cells is more severe than for low specific energy cells.

A represented example without sidewall rupture is Test No. 2 penetrated off-centre from the bottom of the cell. As shown in Fig. 13, some sparks are firstly ejected from the venting holes because battery components start to burn inside the cell under high temperature. The strength of ejection which depended on the internal pressure changed with time. A strong jet of sparks and a weak jet of sparks alternatively presented until the jet fire was generated. The whole process of TR could be divided into three stages. The first stage was spark-dominated, and the second stage was fire-dominated, and the third stage was the cell cooling. Transition between adjacent stages had been reported in our previous study for cells triggered to TR under external heating [55]. In this test, there were no sparks ejected from the penetrating location after nail insertion. But sparks were observed and ejected from the penetrating location in some tests. For tests penetrated from the top cover of the cell, the phenomena were similar, see Fig. A1 (Appendix). The fire behaviour for current used 21700-format cells is more violent than 18650-format cells [28] mainly because more energy is stored in 21700-format cells. Note that it showed some differences in fire behaviour even under the same testing conditions because fire behaviour is complicated and affected by many factors such as heat generation, internal pressure, released gas composition, and external environment.

The fire-burst behaviour from the side of the cell was observed for some tests penetrated from the top cover of the cell as well as from the bottom of the cell. A represented example is Test No. 4 penetrated from the centre of the cell bottom with a nail diameter of 4 mm. As shown in Fig. 14, a lot of sparks are ejected from the side of the cell and at the

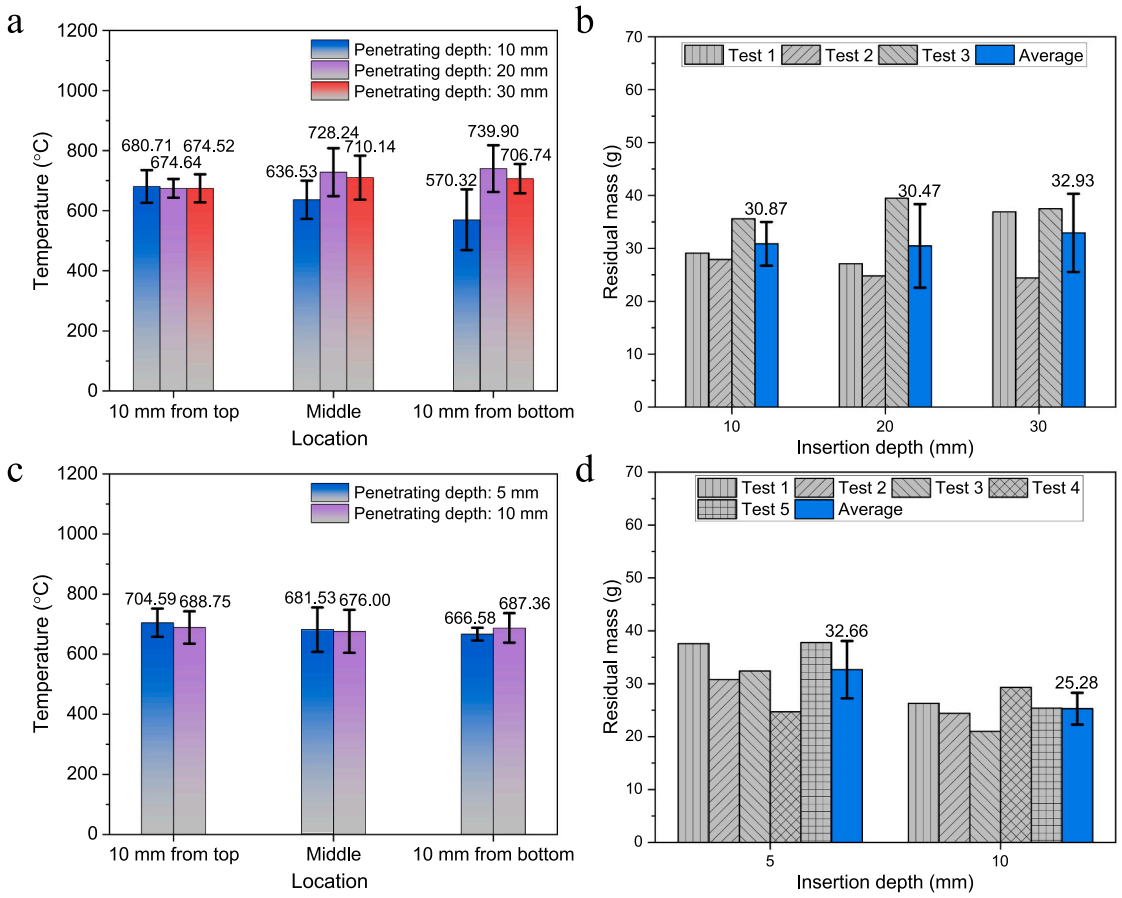

Fig. 10. Comparison of the mean maximum temperature at different measuring points and the mean residual mass of cells with different penetrating depths, penetrated from the centre of the cell bottom (a) and (b), and off-centre from the cell bottom (c) and (d).

same time a few sparks are ejected from the penetrating location after nail insertion. The process of battery combustion was lasted for about 5 mins and initially a jet of fire with sparks was sprayed outside lasting for about 110 s at a certain strength, after that a cluster of fire without sparks was generated and became weak gradually until the fire went out. There were no smoke, gases and sparks discharged from the venting holes. The top cover of the cell is still in relatively good condition, as presented in Fig. 9a, only a small melting spot is found on the top disk after the test. For tests penetrated from the top cover of the cell, the fire-burst behaviour was similar with that penetrated from the cell bottom, see Fig. A2 (Appendix).

3.7. Thermal runaway and sidewall rupture

TR can be characterised by some key indicators such as TR trigger temperature, TR maximum temperature, mass loss ratio, and heat release rate. Observing the change in internal structure of the cell is also a good indicator to characterise TR. To further understand the mechanism of TR and sidewall rupture, an X-ray computed tomography (CT) was used to observe the internal structure after tests. In this work, six cells with 100% SoC after test as listed in Table 3 were scanned by the X-ray CT (TESCAN UniTom XL, Czech Republic) with an exposure voltage of 180 kV, an exposure power of 30.0 W, and an exposure time of 0.85 s to generate 3698 projections with a voxel size of 40 μm. Software (Acquila, Czech Republic and VG Studio Max 2.2, Germany) was used to reconstruct the individual radiographic scans.

Fig. 15 presents slice images of Test No. 4 at 100% SoC penetrated at a speed of 100 mm/s (test condition 10 in Table 3) in the longitudinal direction at different angles (0°, 45°, 90°, and 135°) and in the radial direction at different heights (5 mm, 15 mm, 35 mm, and 65 mm) from the cell base to the cell top, respectively. The visual image of this cell is shown in Fig. 15a and f. The shape of battery casing became very irregular after sidewall rupture. A large crack along the longitudinal direction of the cell can be seen and the top cover of the cell is still in relatively good condition. As shown in Fig. 15, the electrode assembly around the nail tip is damaged severely but other region around the nail keeps good contact. It suggests that internal short circuit mainly occurred in the region around the nail tip at the early stage of nail penetration, then propagated to other regions. The electrode assembly close to the battery core was easy to damage than those close to battery casing because of less constraint and violent chemical reaction in the region close to the battery core. Note that there is no tube/mandrel in this cell. Debris was full of battery core area due to internal airflow. There were many metal particles with different sizes spreading all over electrode materials. These brighter particles are possibly melted aluminium current collector and can be observed on the surface of crack part in Fig. 15a. There was a large amount of residue and molten debris attached to the inner casing of the cell, which may be mainly components of sparks and other products sprayed on the inner surface of battery casing.

Fig. 16 presents slice images of Test No. 1 at 100% SoC penetrated at a speed of 6 mm/s and with a nail diameter of 8 mm (test condition 8 in Table 3) in the longitudinal direction at different angles (0°, 45°, 90°, and 135°) and in the radial direction at different heights (5 mm, 15 mm, 35 mm, and 65 mm) from the cell base to the cell top, respectively. The visual image of this cell is shown in Fig. 16a and f. A long crack and a

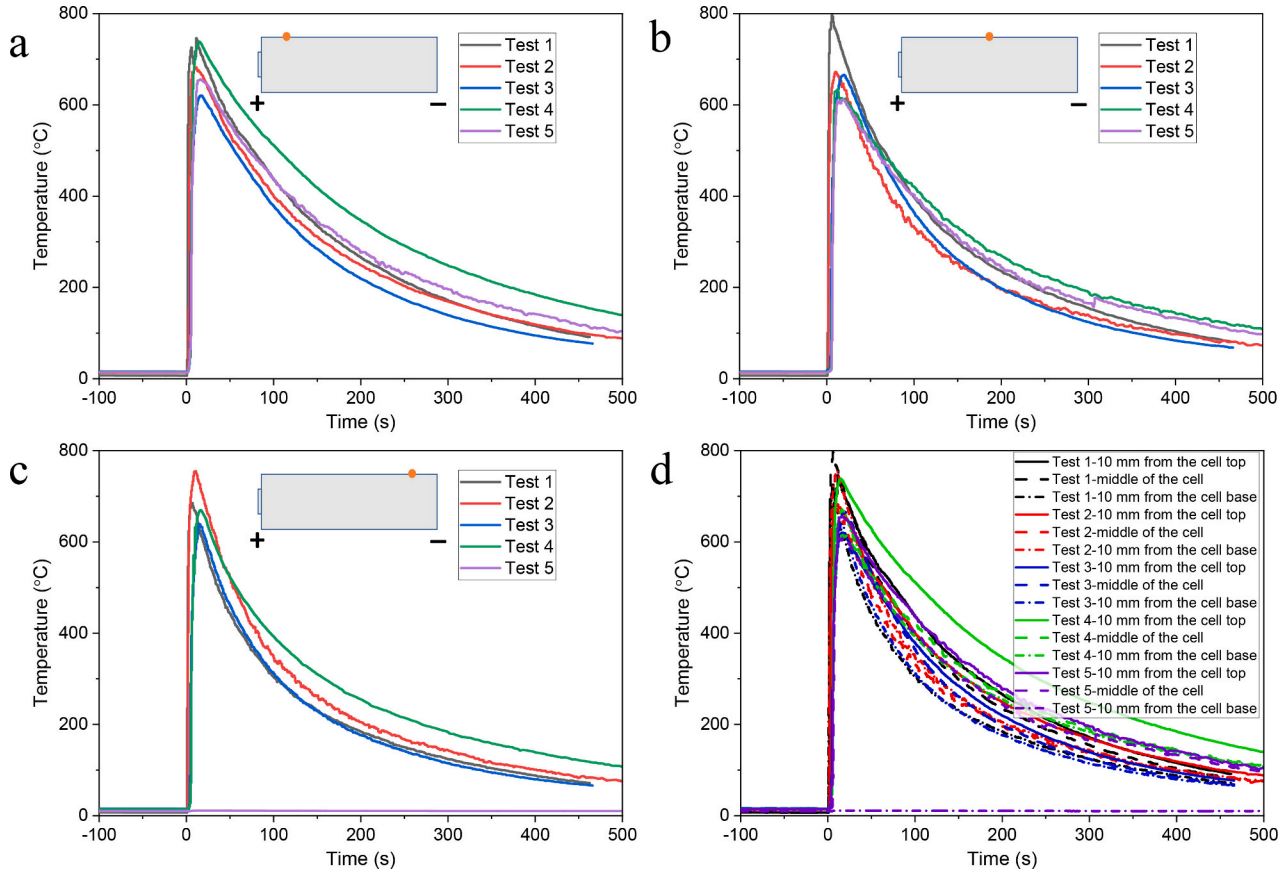

Fig. 11. Temperature profiles at different locations of 100% SoC cells penetrated off-centre from the cell bottom with penetrating depth of 10 mm. (a) 10 mm from the cell top, (b) middle of the cell, (c) 10 mm from the cell base, and (d) three different locations together.

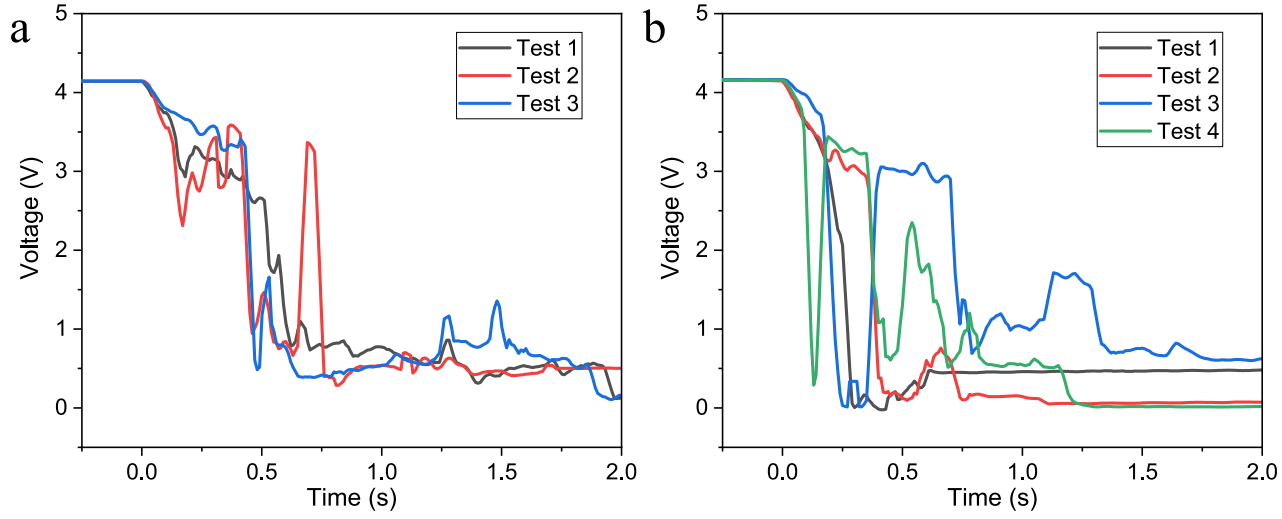

Fig. 12. Voltage profile of the cell penetrated from the centre of the cell bottom with the penetrating depth of 30 mm (a) and off-centre from the cell bottom with the penetrating depth of 10 mm (b).

short crack are generated on the casing. The electrode assembly close to the cell core was firstly damaged by nail because the diameter of nail was more twice than the diameter of mandrel, then the electrode materials around the nail tip were shorted and heat generated, and gases were released. Sidewall rupture happened in this cell under combined effects of high internal pressure, high temperature, and malfunction of the venting disk. As shown in Fig. 16f, venting holes are damaged and there is only a hole pierced by the nail. In addition, there are no additional vents generated on the positive terminal of the cell. A cavity was generated in the upper part of the cell because the pressure generated by gases and the nail pushed and moved the electrode assembly forwards. A large cavity was also formed in the low part of the cell. Similar to the phenomena presented in Fig. 15, there were some melted aluminium particles with different sizes spreading all over electrode materials and lots of molten fragments attached to electrode materials and the inner case in the low part of the cell.

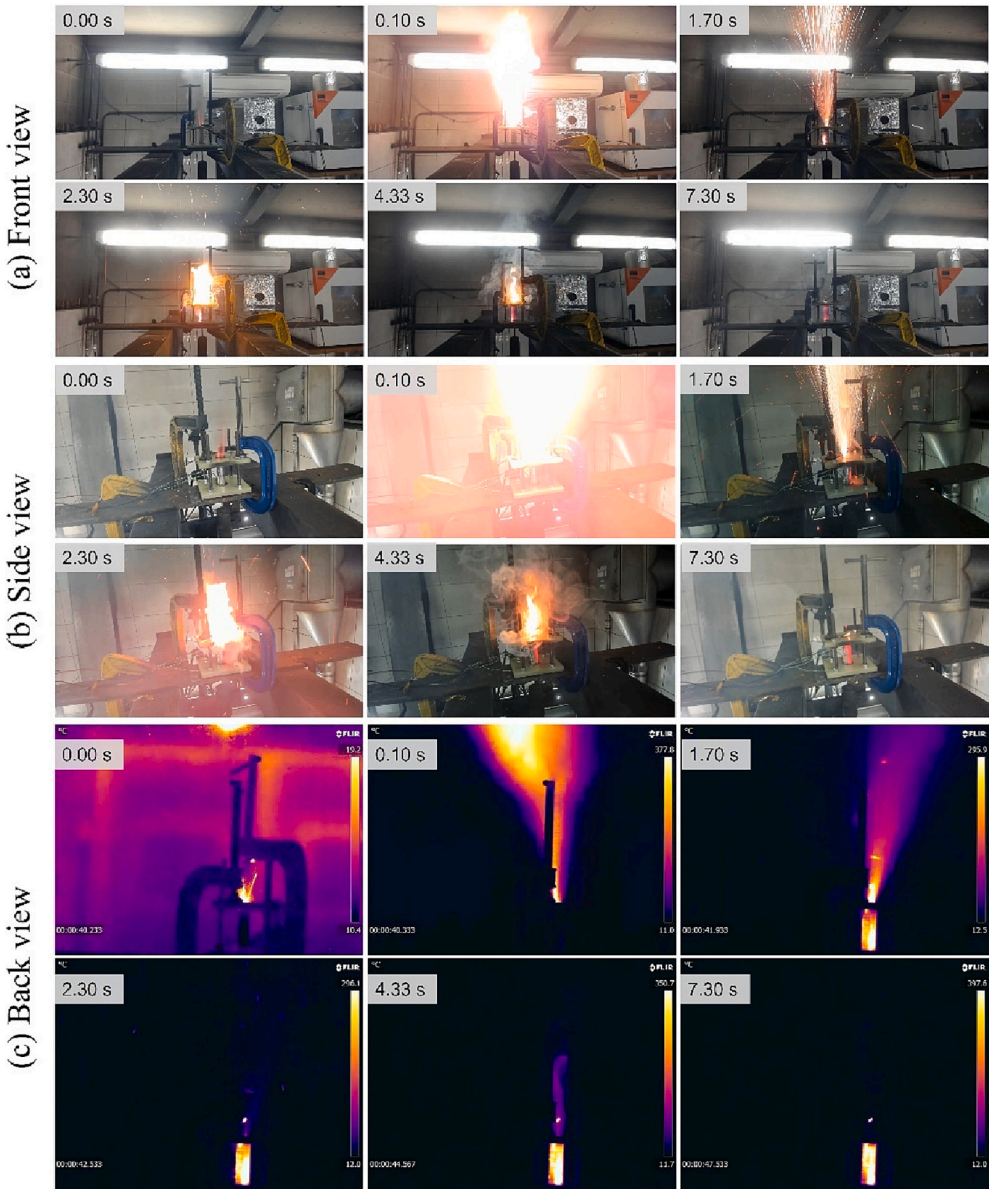

Fig. 13. Evolution of fire behaviour for Test No. 2 at 100% SoC penetrated off-centre from the cell bottom with a penetrating depth of 5 mm (test condition 16 in Table 3). (a) Front view, (b) side view, and (c) back view from IR camera.

To compare the internal structure of cells without experiencing sidewall rupture during nail penetration, as shown in Fig. 17, four cells listed in Table 3 with different testing conditions were scanned by CT. The common features of these CT images were melting aluminium particles spreading over battery electrodes, and the electrode assembly was in a disorder state and most of the electrode materials were broken into pieces under internal airflow. Fig. 17a presents the Test No. 1 pierced from the top cover of the cell at a speed of 0.5 mm/s (test condition 9 in Table 3). The collapse in the upper part of the cell was observed. This phenomenon is less common, and the possible reason is that at high temperature the strength of the cell casing drops beyond the point when it cannot support the structural integrity. Especially if the internal pressure decreased quickly and fell below the atmospheric pressure. This is possibly occurred when a large amount of gas is discharged from venting holes in a very short time, creating a vacuum inside the cell. The cavity was detected by CT scan, which indicates to the occurrence of such vacuum. Two melting aluminium balls were attached on the top cover of the cell after test. These balls were from the inside of the cell and went outside via the venting hole. A lot of melting aluminium particles with different sizes and brighter colour could be found inside the cell, as shown in Fig. 17a. Fig. 17b presents the Test No. 1 with off-centre penetration from the cell bottom and with the penetrating depth of 10 mm (test condition 17 in Table 3). A large cavity was generated inside the cell and the negative tab with a long and white line shape was detached from the cell bottom due to damage during nail penetration. For tests penetrated from the centre of the cell bottom with two different nail diameters, as shown in Fig. 17c (test condition 14 in Table 3) and 17d (test condition 12 in Table 3), a lot of residues accumulated under the top cover of the cell. The components of the residue possibly be sparks but were blocked by the top cover of the cell when ejecting from the cell. The top cover of the cell was partly melted under high temperature. These CT scan images show that the venting disk played an important role in sidewall rupture.

Based on our test results, sidewall rupture of the cell was influenced by many factors which included the penetrating depth of the nail, the nail speed, the nail diameter, the penetrating location, and the cell SoC.

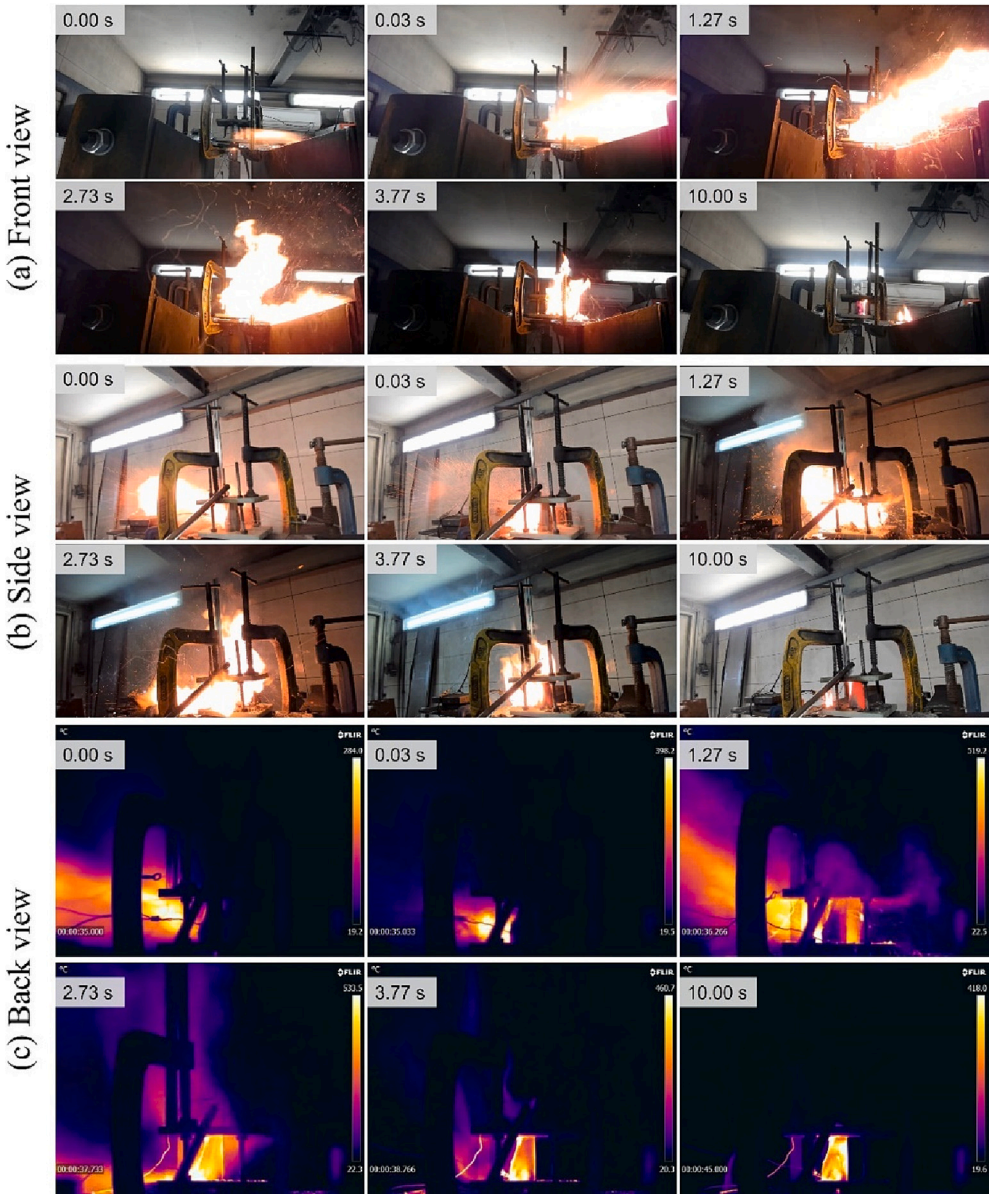

Fig. 14. Evolution of fire behaviour for Test No. 4 at 100% SoC penetrated from the centre of the cell bottom with a nail diameter of 4 mm (test condition 11 in Table 3). (a) Front view, (b) side view, and (c) back view from IR camera.

The likelihood of sidewall rupture increased with the increasement of nail speed, nail diameter, penetrating depth and SoC. Penetrating from the top cover of the cell was easier to cause sidewall rupture than from the bottom of the cell. As shown in Fig. 18, sidewall rupture is mainly influenced by the casing strength, internal pressure, and the opening area of the venting disk.

The casing strength for the given material depends on its strength under high temperature and the thickness of the casing. As reported by Lao et al. [10], the tensile strength of casing material monotonously decreases with the increasing temperature, and the tensile strength at 800 °C drops to 5% of that at room temperature. The high temperature influenced not only the casing strength, but also the thickness. The previous study showed that there is an 12.7% reduction in casing thickness compared with the fresh cell by CT scan [17]. Reduction in thickness [58] and drop in tensile strength under high temperature lead to the decline in casing strength. The internal pressure depends on the gases released, internal space, and internal temperature. The gases released are directly related to battery components, SoC, and heat generation. A cell with high SoC stores more energy than a low SoC, which means that the exothermic reaction for a high-SoC cell is more violent than a low-SoC cell and therefore more energy will be released for a high-SoC cell. The more internal space is occupied by the thicker nail and deeper insertion. According to the ideal gas law, the internal pressure is also related to the internal temperature, which depends on the heat generation inside the cell. The opening area of venting disk also plays an important role in sidewall rupture. The venting disk may not be open even the pressure inside the cell is greater than the given value if the venting disk has a manufacturing defect, manufacturing error, or the venting disk is damaged by the nail during penetration from the top cover of the cell. All of them can lead to malfunction of the venting disk, and therefore leading to the decrease in the opening area of the venting disk, which further increases the risk of sidewall rupture. For example, some tests, see Fig. 9a and Fig. 15f, showed that sidewall rupture happened but the top cover of the cell was still in relatively good condition.

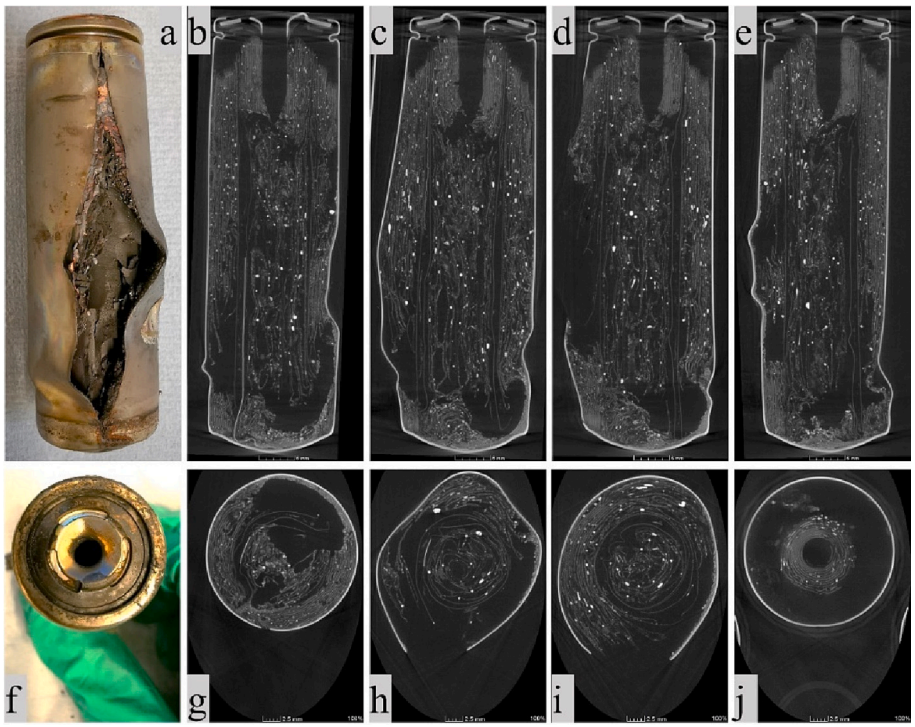

Fig. 15. Internal structure of Test No. 4 at 100% SoC penetrated at a speed of 100 mm/s (test condition 10 in Table 3). Photos after test from side view (a) and top view (f) and slice images in the longitudinal direction at different angles (0°, 45°, 90°, and 135°) (b)-(e) and in the radial direction at different heights (5 mm, 15 mm, 35 mm, and 65 mm) (g)-(j) from the cell base to the cell top.

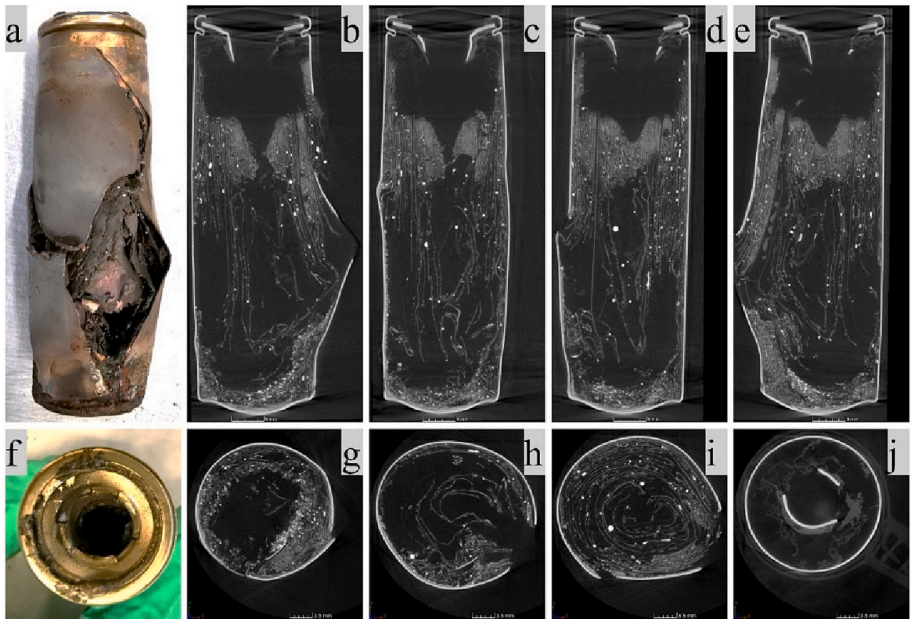

Fig. 16. Internal structure of Test No. 1 at 100% SoC penetrated at a speed of 6 mm/s and with a nail diameter of 8 mm (test condition 8 in Table 3). Photos after test from side view (a) and top view (f) and slice images in the longitudinal direction at different angles (0°, 45°, 90°, and 135°) (b)-(e) and in the radial direction at different heights (5 mm, 15 mm, 35 mm, and 65 mm) (g)-(j) from the cell base to the cell top.

4. Conclusions

The behaviour of TR and sidewall rupture of high specific energy 21700-format LIBs under nail penetration were studied by a series of tests. The results of post-mortem analysis and CT scan have provided an insight to understand the mechanism of sidewall rupture and TR.

The mean maximum temperature at different measuring points is not greatly influenced by those penetrating parameters. The mean mass loss ratio of the cell with 100% SoC is greater than 45% under each test condition listed in Table 3, and the maximum of them is as high as 62.5% when penetrating off-centre from the cell bottom and with a penetrating depth of 10 mm, but sidewall rupture is not observed, suggesting that

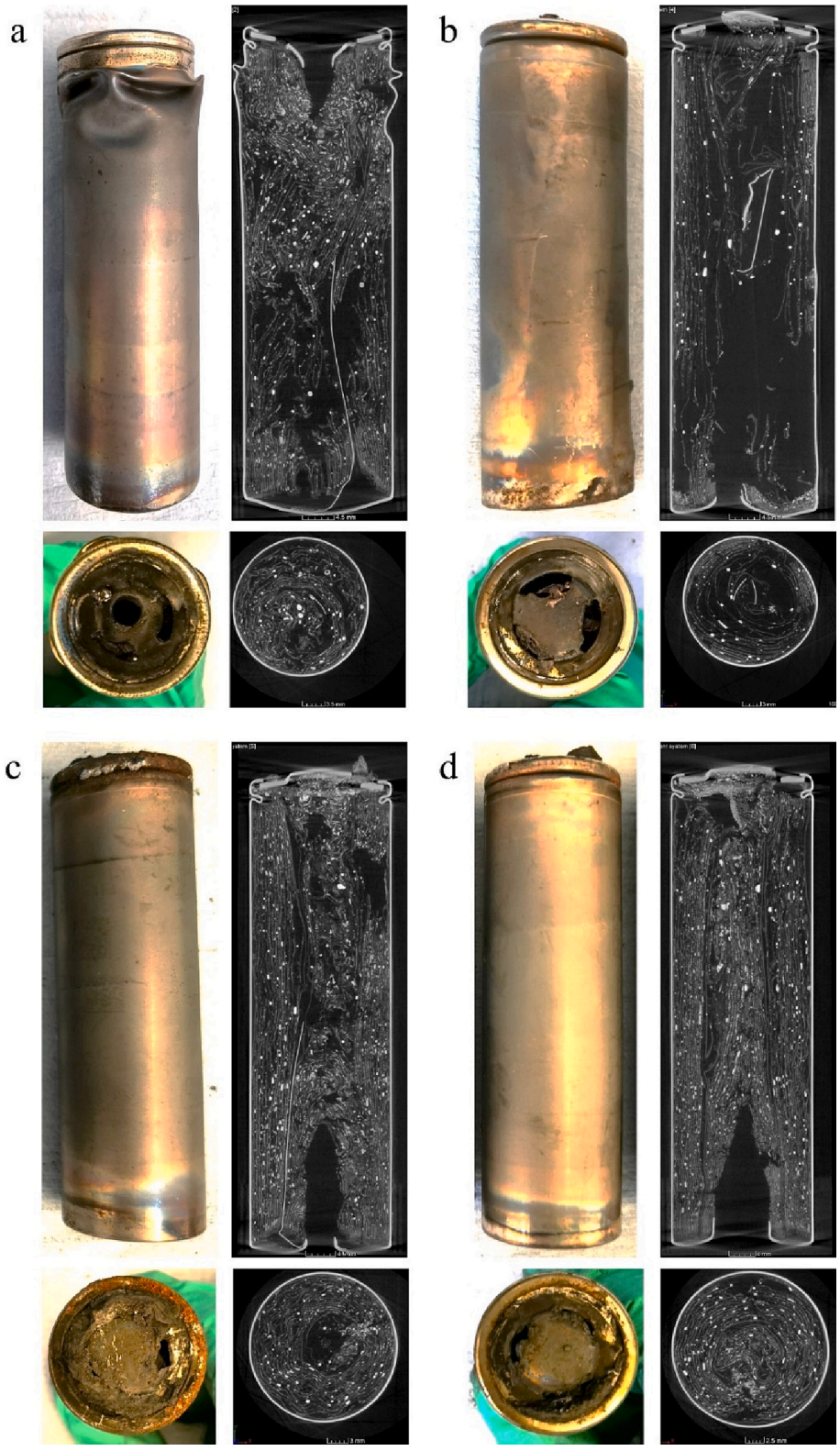

Fig. 17. Internal structure of cells without sidewall rupture. (a) Test No. 1 at 100% SoC penetrated from the centre of the cell bottom at a speed of 0.5 mm/s and with a nail diameter of 4 mm (test condition 9 in Table 3), (b) Test No. 1 at 100% SoC penetrated off-centre from the cell bottom at a speed of 6 mm/s and with a nail diameter of 4 mm and the penetrating depth of 10 mm (test condition 17 in Table 3), (c) Test No. 3 at 100% SoC penetrated from the centre of the cell bottom at a speed of 6 mm/s and with a nail diameter of 4 mm and the penetrating depth of 20 mm (test condition 14 in Table 3), and (d) Test No. 3 at 100% SoC penetrated from the centre of the cell bottom at a speed of 6 mm/s and with a nail diameter of 8 mm and the penetrating depth of 20 mm (test condition 12 in Table 3).

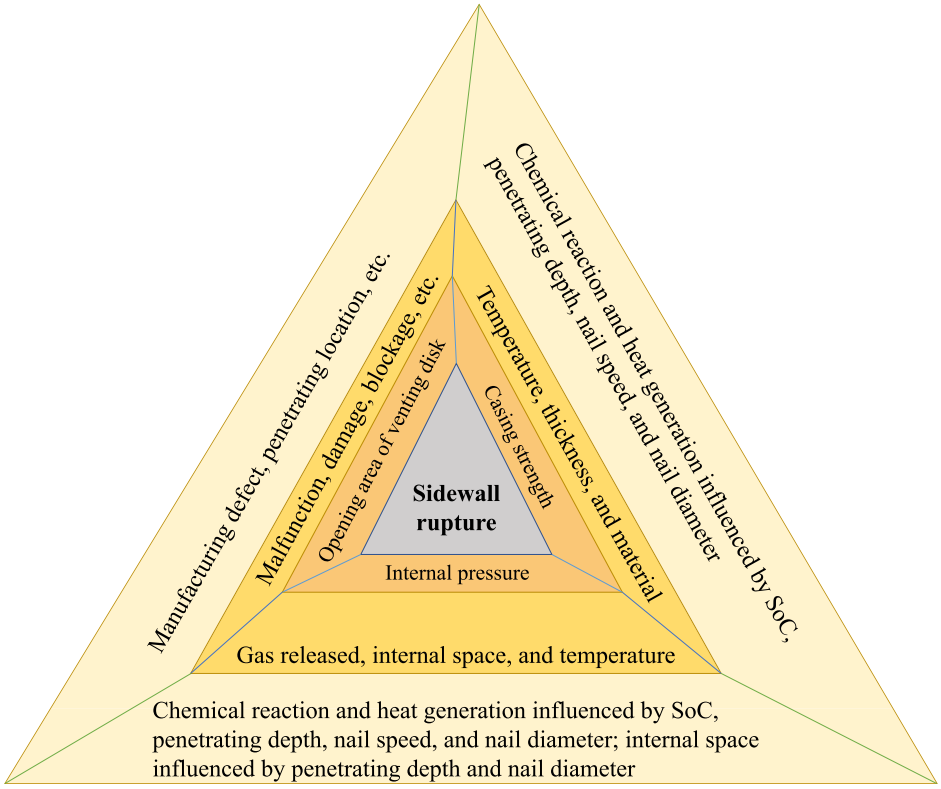

Fig. 18. Influencing factors of sidewall rupture of lithium-ion batteries.

the internal pressure releases slightly slower than testing conditions with sidewall rupture. The likelihood of sidewall rupture increases with the increasing nail speed, nail diameter, penetrating depth and state of charge when penetrating from the top cover of the cell. While the likelihood of sidewall rupture is little affected by the penetrating depth and nail diameter for penetrating from the bottom of the cell because only one test happened sidewall rupture due to malfunction of the venting disk. The casing strength, internal pressure, and the opening area of the venting disk are main factors which determine the sidewall rupture of the cell or not. The results showed that the risk of sidewall rupture increases greatly if the venting disk does not work due to malfunction, blockage, and damage, etc. Therefore, adding a venting disk at the bottom of the cell may increase the battery safety and reduce the risk of sidewall rupture. Two typical fire-burst behaviours were observed based on cells with or without sidewall rupture. More attention should be paid to the fire burst from the side of the cell because the flame directly heats the adjacent cells if there are no mitigation materials between cells. In addition, penetrating off-centre from the bottom of the cell with a thin nail and lower speed could provide relatively good reproducibility of TR results. Note that the main conclusions are made based on 21700-format cells with lithium nickel cobalt aluminium oxide cathode and are therefore not universal because the sidewall rupture behaviour is influenced by many factors. But this work can provide a reference for analysing the sidewall rupture behaviour of cylindrical cells. Putting a pressure sensor inside the cell would be a future work to investigate the changes in internal pressure during TR.

The volume-averaged properties of battery component are popularly used in current modelling study of TR. The current work will help understand the mechanism of TR and sidewall rupture of the cell under mechanical abuse conditions. The insight of fire behaviour, temperature, residual mass, and internal structure of cell will help for the development of a more accurate model in predicting TR and sidewall rupture of the cell.

CRediT authorship contribution statement

Haodong Chen: Writing – review & editing, Writing – original draft, Visualization, Software, Methodology, Investigation, Formal analysis, Data curation, Conceptualization. **Evangelos Kalamaras:** Methodology, Investigation. **Ahmed Abaza:** Methodology, Investigation. **Yashraj Tripathy:** Methodology, Investigation. **Jason Page:** Investigation. **Anup Barai:** Writing – review & editing, Methodology, Investigation, Funding acquisition, Conceptualization.

Declaration of Competing Interest

The authors declare that they have no known competing financial interests or personal relationships that could have appeared to influence the work reported in this paper.

Data availability

Data will be made available on request.

Acknowledgements

The research presented within this paper is supported by the Jaguar Land Rover Catapult project and the Faraday Institution “SafeBatt – Science of Battery Safety” [FIRG028]. The research was undertaken in collaboration with the WMG Centre High Value Manufacturing Catapult (funded by Innovate UK) and Jaguar Land Rover. The X-ray CT was done in the National Facility for X-Ray Computed Tomography (NXCT) and the Centre for Imaging, Metrology, and Additive Technologies (CiMAT) at the University of Warwick, funded by ESPRC project number: EP/T02593X/1.

Appendix A

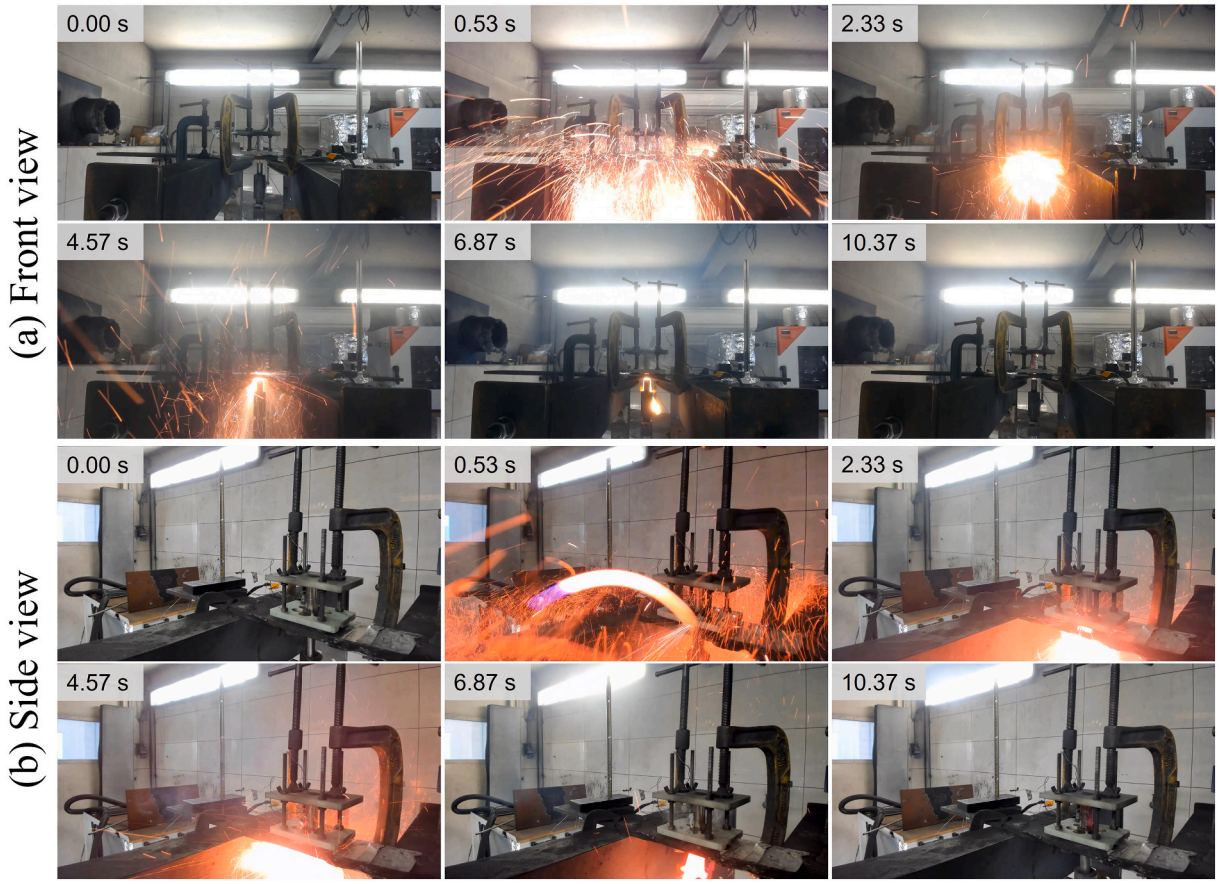

Fig. A1. Evolution of fire behaviour of Test No. 1 at 100% SoC penetrated from the top cover of the cell with a nail diameter of 3 mm (test condition 7 in Table 3). (a) Front view, and (b) side view.

Fig. A2. Evolution of fire behaviour of Test No. 1 at 100% SoC penetrated from the top cover of the cell with a nail diameter of 4 mm and at a speed of 100 mm/s (test condition 10 in Table 3). (a) Front view, (b) side view, and (c) back view from IR camera.

References

[1] Bodine R. In: Brennan R, editor. Gas vs. electric car fires [2022 findings]. AutoinsuranceEZ; 2022.
[2] Schäfer AW, Barrett SRH, Doyme K, Dray LM, Gnadt AR, Self R, et al. Technological, economic and environmental prospects of all-electric aircraft. Nat Energy 2018;4:160–6.
[3] ATI. In: Institute AT, editor. Accelerating ambition - Technology strategy 2019; 2019.
[4] Authority UCA. In: URA Innovation, editor. Towards net XZero aviation - UK legislation framework. Innovation Hub; 2021.
[5] Bezard C, Goodwin I, Tofighi-Niaki P, Rohrbach P. Lithium batteries: Safe to fly? Airbus; 2016.
[6] Wang Q, Ping P, Zhao X, Chu G, Sun J, Chen C. Thermal runaway caused fire and explosion of lithium ion battery. J Power Sources 2012;208:210–24.
[7] Wang Q, Mao B, Stoliarov SI, Sun J. A review of lithium ion battery failure mechanisms and fire prevention strategies. Prog Energy Combust Sci 2019;73:95–131.

[8] Mauger A, Julien C. Critical review on lithium-ion batteries: are they safe? Sustainable? Ionics. 2017;23:1933–47.
[9] Feng X, Ren D, He X, Ouyang M. Mitigating thermal runaway of lithium-ion batteries. Joule. 2020;4:743–70.
[10] Lao L, Su Y, Zhang Q, Wu S. Thermal runaway induced casing rupture: formation mechanism and effect on propagation in cylindrical lithium ion battery module. J Electrochem Soc 2020;167:090519.
[11] Anderson N, Tran M, Darcy E. 18650 cell bottom vent: preliminary evaluation into its merits for preventing side wall rupture. In: Proc S&T meeting; 2016. p. 1–53.
[12] Kong L, Hu X, Gui G, Su Y, Pecht M. Computed tomography analysis of li-ion battery case ruptures. Fire Technol 2020;56:2565–78.
[13] Finegan DP, Darcy E, Keyser M, Tjaden B, Heenan TMM, Jervis R, et al. Identifying the cause of rupture of Li-ion batteries during thermal runaway. Adv Sci 2018;5:1700369.
[14] Finegan DP, Darcy E, Keyser M, Tjaden B, Heenan TMM, Jervis R, et al. Characterising thermal runaway within lithium-ion cells by inducing and monitoring internal short circuits. Energ Environ Sci 2017;10:1377–88.
[15] Jia Y, Darst J, Surelia A, Delafuente D, Finegan DP, Xu J. Deformation and fracture behaviors of cylindrical battery shell during thermal runaway. J Power Sources 2022;539:231607.
[16] Zhu Y-l, Wang C-j, Gao F, Shan M-x, Zhao P-l, Meng Q-f, et al. Rupture and combustion characteristics of lithium-ion battery under overcharge. J Energy Storage 2021;38:102571.
[17] Chen H, Kalamaras E, Abaza A, Tripathy Y, Page J, Barai A. Experimental study of sidewall rupture of cylindrical Lithium-ion batteries under radial nail penetration. J Electrochem Soc 2022;169:120528.
[18] Liu L, Feng X, Zhang M, Lu L, Han X, He X, et al. Comparative study on substitute triggering approaches for internal short circuit in lithium-ion batteries. Appl Energy 2020;259:114143.
[19] Essl C, Golubkov A, Fuchs A. Comparing different thermal runaway triggers for two automotive lithium-ion battery cell types. J Electrochem Soc 2020;167:130542.
[20] Feng X, He X, Ouyang M, Lu L, Wu P, Kulp C, et al. Thermal runaway propagation model for designing a safer battery pack with 25 ah $LiNi_xCo_yMn_zO_2$ large format lithium ion battery. Appl Energy 2015;154:74–91.
[21] Feng X, Sun J, Ouyang M, Wang F, He X, Lu L, et al. Characterization of penetration induced thermal runaway propagation process within a large format lithium ion battery module. J Power Sources 2015;275:261–73.
[22] Lamb J, Orendorff CJ, Steele LAM, Spangler SW. Failure propagation in multi-cell lithium ion batteries. J Power Sources 2015;283:517–23.
[23] Ruiz V, Pfrang A, Kriston A, Omar N, Van den Bossche P, Boon-Brett L. A review of international abuse testing standards and regulations for lithium ion batteries in electric and hybrid electric vehicles. Renew Sustain Energy Rev 2018;81:1427–52.
[24] Abaza A, Ferrari S, Wong HK, Lyness C, Moore A, Weaving J, et al. Experimental study of internal and external short circuits of commercial automotive pouch lithium-ion cells. J Energy Storage 2018;16:211–7.
[25] Diekmann J, Doose S, Weber S, Munch S, Haselrieder W, Kwade A. Development of a new procedure for nail penetration of lithium-ion cells to obtain meaningful and reproducible results. J Electrochem Soc 2020;167:090504.
[26] Wang J, Mei W, Cui Z, Dong D, Shen W, Hong J, et al. Investigation of the thermal performance in lithium-ion cells during polyformaldehyde nail penetration. J Therm Anal Calorim 2021;145:3255–68.
[27] Ma T, Chen L, Liu S, Zhang Z, Xiao S, Fan B, et al. Mechanics-morphologic coupling studies of commercialized lithium-ion batteries under nail penetration test. J Power Sources 2019;437:226928.
[28] Mao B, Chen H, Cui Z, Wu T, Wang Q. Failure mechanism of the lithium ion battery during nail penetration. Int J Heat Mass Transf 2018;122:1103–15.
[29] Xu J, Mei W, Zhao C, Liu Y, Zhang L, Wang Q. Study on thermal runaway mechanism of 1000 mAh lithium ion pouch cell during nail penetration. J Therm Anal Calorim 2021;144:273–84.
[30] Wang J, Mei W, Cui Z, Shen W, Duan Q, Jin Y, et al. Experimental and numerical study on penetration-induced internal short-circuit of lithium-ion cell. Appl Therm Eng 2020;171:115082.
[31] Reichert M, Haetge J, Berghus D, Wendt C, Meier V, Rodehorst U, et al. Lithium-ion cell nail penetration safety experiments under adiabatic conditions. ECS Trans 2014;61:87–103.
[32] Perea A, Paolella A, Dube J, Champagne D, Mauger A, Zaghib K. State of charge influence on thermal reactions and abuse tests in commercial lithium-ion cells. J Power Sources 2018;399:392–7.
[33] Sharp M, Darst J, Hughes P, Billman J, Pham M, Petrushenko D, et al. Thermal runaway of Li-ion cells: how internal dynamics, mass ejection, and heat vary with cell geometry and abuse type. J Electrochem Soc 2022;202:169. 020526.
[34] Yokoshima T, Mukoyama D, Maeda F, Osaka T, Takazawa K, Egusa S, et al. Direct observation of internal state of thermal runaway in lithium ion battery during nail-penetration test. J Power Sources 2018;393:67–74.
[35] Huang S, Du XN, Richter M, Ford J, Cavalheiro GM, Du ZJ, et al. Understanding Li-ion cell internal short circuit and thermal runaway through small, slow and in situ sensing nail penetration. J Electrochem Soc 2020;167:090526.
[36] Doose S, Haselrieder W, Kwade A. Effects of the nail geometry and humidity on the nail penetration of high-energy density lithium ion batteries. Batteries. 2021;7:6.
[37] Huang Z, Li H, Mei W, Zhao C, Sun J, Wang Q. Thermal runaway behavior of lithium iron phosphate battery during penetration. Fire Technol 2020;56:2405–26.
[38] Chen MJ, Ye Q, Shi CM, Cheng Q, Qie BY, Liao XB, et al. New insights into nail penetration of Li-ion batteries: effects of heterogeneous contact resistance. Batter Supercaps 2019;2:874–81.
[39] Zhao W, Luo G, Wang C-Y. Modeling nail penetration process in large-format Li-ion cells. J Electrochem Soc 2015;162. A207-A217.
[40] SAE J2464. Electric and hybrid electric vehicle rechargeable energy storage system (RESS) safety and abuse testing. 2009.
[41] GB 38031-2020. Electric vehicles traction battery safety requirements. 2020.
[42] Liu B, Yin S, Xu J. Integrated computation model of lithium-ion battery subject to nail penetration. Appl Energy 2016;183:278–89.
[43] Finegan DP, Tjaden B, Heenan TMM, Jervis R, Di Michiel M, Rack A, et al. Tracking internal temperature and structural dynamics during nail penetration of lithium-ion cells. J Electrochem Soc 2017;164. A3285-A3291.
[44] Chiu K-C, Lin C-H, Yeh S-F, Lin Y-H, Chen K-C. An electrochemical modeling of lithium-ion battery nail penetration. J Power Sources 2014;251:254–63.
[45] Liang G, Zhang Y, Han Q, Liu Z, Jiang Z, Tian S. A novel 3D-layered electrochemical-thermal coupled model strategy for the nail-penetration process simulation. J Power Sources 2017;342:836–45.
[46] Zhao R, Liu J, Gu J. A comprehensive study on Li-ion battery nail penetrations and the possible solutions. Energy. 2017;123:392–401.
[47] Vyroubal P, Kazda T. Finite element model of nail penetration into lithium ion battery. J Energy Storage 2018;20:451–8.
[48] Yamanaka T, Takagishi Y, Tozuka Y, Yamaue T. Modeling lithium ion battery nail penetration tests and quantitative evaluation of the degree of combustion risk. J Power Sources 2019;416:132–40.
[49] Chen M, Bai F, Lin S, Song W, Li Y, Feng Z. Performance and safety protection of internal short circuit in lithium-ion battery based on a multilayer electro-thermal coupling model. Appl Therm Eng 2019;146:775–84.
[50] Doyle M, Fuller TF, Newman J. Modeling of galvanostatic charge and discharge of the lithium/polymer/insertion cell. J Electrochem Soc 1993;140:1526–33.
[51] Fuller TF, Doyle M, Newman J. Simulation and optimization of the dual lithium ion insertion cell. J Electrochem Soc 1994;141:1–10.
[52] Kim G-H, Pesaran A, Spotnitz R. A three-dimensional thermal abuse model for lithium-ion cells. J Power Sources 2007;170:476–89.
[53] Hatchard TD, MacNeil DD, Basu A, Dahn JR. Thermal model of cylindrical and prismatic lithium-ion cells. J Electrochem Soc 2001;148:A755-A761.
[54] Quinn JB, Waldmann T, Richter K, Kasper M, Wohlfahrt-Mehrens M. Energy density of cylindrical Li-ion cells: a comparison of commercial 18650 to the 21700 cells. J Electrochem Soc 2018;165. A3284-A3291.
[55] Chen H, Buston JEH, Gill J, Howard D, Williams RCE, Rao Vendra CM, et al. An experimental study on thermal runaway characteristics of lithium-ion batteries with high specific energy and prediction of heat release rate. J Power Sources 2020;472:228585.
[56] Shelke AV, Buston JE, Gill J, Howard D, Abbott KC, Goddard SL, et al. Characterizing and predicting 21700 NMC lithium-ion battery thermal runaway induced by nail penetration. Appl Therm Eng 2022;209:118278.
[57] Wang Q, Sun J, Yao X, Chen C. Thermal behavior of lithiated graphite with electrolyte in lithium-ion batteries. J Electrochem Soc 2006;153:A329-A333.
[58] Roylance D. Pressure vessels. Cambridge: Department of Materials Science and Engineering, Massachusetts Institute of Technology; 2001.